INTERNATIONAL JOURNAL OF AUTOMOTIVE AND MECHANICAL ENGINEERING
ISSN: 2229-8649 e-ISSN: 2180-1606
VOLUME 22, ISSUE 2, 2025, 12443 - 12467
DOI: https://doi.org/10.15282/ijame.22.2.2025.15.0952

RESEARCH ARTICLE

Modeling and Contact Stress Analysis of Crossed-Axes Helical Gear System

Mohammed Abdulaal Kadhim*, Mohammad Qasim Abdullah

Mechanical Engineering Department, College of Engineering, University of Baghdad, Iraq

ABSTRACT – Crossed helical gears are susceptible to pitting damage resulting from contact stress, primarily due to the theoretical point of contact between the gears. The contact point transforms into an ellipse due to the deformation of the elastic material under varying loading conditions. The overheating between the tooth profiles during the engagement process contributes to the proliferation of pits, deteriorating the tooth surface and causing premature tooth failure. This study investigates the influence of two modifications: the tip relief design and the compound profile design, which combines involute and epicycloid profiles. A shaping process generates both standard and modified helical gears. The results indicate that increasing the amount of misalignment with a smaller harmonic waveform reduces the transmission error. The involute-epicycloid profile reduces the sliding velocity with the most significant improvement of approximately 16%. A decrease in the angle of pressure and an increase in the helix angle of 1.5 and 1.7, respectively, enhance the total contact ratio. The maximum contact stress observed for the modified involute-epicycloid surface decreased by 6%, 6%, and 2%, while the tooth root stress reduced by 6%, 8%, and 12% for the three positions, respectively. Meanwhile, the maximum contact stress for tip relief modification decreased by 2%, 6%, and -6%, whereas the tooth root stress reduced by 2%, 7%, and -1% for the three positions, respectively. Consequently, the modified crossed helical gear drive demonstrates superior performance compared to the standard gear drive for a given helix angle. Furthermore, the stress concentration factor decreased through the use of the modified helical teeth by about 2% and 6%.

ARTICLE HISTORY

Received	:	30th May 2024
Revised	:	07th Mar. 2025
Accepted	:	21st May 2025
Published	:	27th June 2025

KEYWORDS

Helical gear
Crossed-axes helical gear
Tip relief
Epicycloid
Contact stress
Tooth root stress

1. INTRODUCTION

Gears are cylindrical wheels equipped with teeth that are designed to facilitate the transfer of mechanical power between rotating shafts. The gear wheel represents a gearing system that has captured the interest of numerous engineers due to the various technological challenges associated with meshing. Gears can be classified into many general categories depending on the orientation of the shaft axes: parallel axes, non-parallel intersecting axes, and non-parallel non-intersecting axes. Crossed helical gears, referred to as crossed-axes helical gears, resemble regular helical gears but are mounted on non-parallel shafts and non-coplanar, featuring non-intersecting axes [1]. The relationship between the crossing angle $\boldsymbol{\lambda}$ and the helix angle $\boldsymbol{\beta_i}$ $(i = 1, 2)$ of mating gears is:

$$\lambda = \beta_1 + \beta_2 \tag{1}$$

Helical gears typically feature helicoid surfaces that are oriented in the same direction. A smaller helix angle is utilized in a negative direction. A typical shaft angle ranges from 0 to 90°. This occurs when gears with complementary helix angles are paired, maintaining the same direction of rotation. The operation of crossed helical gears fundamentally differs from that of parallel helical gears, as the engaging teeth slide against one another during rotation. The sliding velocity increases with an increase in the axis angle of rotation, reaching a minimum when the two helix angles are aligned in the same direction. The interaction between the surfaces of paralleled helical gear teeth occurs along a diagonal line, whereas the interaction between the tooth surfaces of crossed helical gear initiates as a point contact, which transforms into an elliptical shape due to elastic deformation under varying loading conditions. Crossed helical gearing, owing to its theoretical point contact, exhibits low load-carrying capacities, typically not exceeding a resultant tooth load of 400 N. Contact ratios of two or more are typically employed to enhance load capacity [2]. It is common to specify lower pressure angle values and relatively large tooth depth values to enhance the ratio of contact. A gear system that incorporates a helical gear represents a specific instance of gearing with crossed screw axes [3]. Numerous research studies have been conducted in this area. Despite the extensive research conducted in this field, the skew involute helical gear system remains a significant concern for designers and manufacturers.

Sankar and Nataraj [4] examined the transmission errors between the driving and driven helical gears, which can result from manufacturing defects or misalignment in the gearbox assembly. These errors lead to noise and vibrations during gearbox operation. To prevent tooth damage in the helical teeth caused by transmission errors, the authors implemented tip relief on the gear tooth and utilized a combination of epicycloid with an involute surface. The study employed finite element analysis (FEA) to evaluate the performance of the existing standard and modified helical gear pairs. The findings

***CORRESPONDING AUTHOR | M.A. Kadhim** | ✉ mohammed.abd2103p@coeng.uobaghdad.edu.iq

indicate that the adjusted design, which incorporates tip relief and modified helical gear, is better than the traditional standard gear for wind generator applications. This is especially pertinent as wind turbine generators experience variable wind forces, abrupt grid failures, and issues with pitching and braking systems.

Natsuhiko et al. [5] employed an involute-cycloid compound tooth configuration for the spur gear. This gear type outperforms the standard spur gear in terms of bending strength, surface durability, and efficiency of power transfer. The study evaluated stresses in the tooth's root and contact area surface of the involute-cycloid compound tooth profile spur gear by modifying design factors, including the radius of rolling circle, angle of pressure, and depth of tooth, which determine the tooth profile. The authors examined the effect of design factors on the strength and driving performance of involute-cycloid composite tooth profile spur gears based on computational results. Additionally, the research assessed the tooth stress of contact and root stress while accounting for the center distance error, as well as analyzed the influence of center distance on the driving performance of involute-cycloid compound tooth profile spur gears based on experimental findings. Zhang and Liang [6] improved the method for manufacturing gears. The theory of gear ensures the basics of the curvilinear tooth gears. The convex and concave tooth surfaces were produced using two separate one-sided face-milling cutters. The line contact was demonstrated in the final curvilinear gear drives that were mesh-generated. The work aimed to define gear drives based on the position of the line contact, namely double-helical gear drives. In addition, the study consisted of three main parts: a comparison of stresses and transmission errors in two-gear drives with identical contact ratios; the derivation of equations for the tooth surface, an analysis of transmission errors, and FEA; and four numerical examples illustrating the advantages and disadvantages of curvilinear cylindrical gear drives.

Liang et al. [7] introduced the curved contact element to the notion of contact and proposed a technique for constructing gear pairs with a short angle. The crossed helical gear unit was modeled mathematically. The stress analysis was carried out using ANSYS software. The FEA was conducted with a shaft angle of 10°, utilizing 3D models of a non-parallel helical gear pair created in MATLAB. The findings indicated that the pinion could withstand a maximum von Mises stress of 793.69 MPa. The involute gear profile pair was used as a point of reference, with the meshing point experiencing a maximum contact stress of 1,639 MPa, which is distributed along the line of contact. The pinion demonstrated the capacity to withstand a von Mises stress of up to 1,233.8 MPa. Wu et al. [8] investigated the technical difficulties associated with high-strength gears. The study addressed the technicalities of transmission design, design and manufacturing integration, processing, and performance assessment of high-strength gears. The research focused on the technical aspects associated with design-manufacturing integration, particularly in wind power generation and aviation engines. The latest findings in anti-fatigue design, manufacture, and service performance assessment of high-strength gears were reviewed to encourage the development and use of high-strength gear technology.

Abdulaal and Abdullah [9] proposed a principle of the method involving the introduction of a contact line rather than a point between two meshing teeth. They employed a modified cutter tool with increased standard pressure angles of 25° and 35°. The design of the non-classic surface aims to prevent interference among the helical teeth. This modification incorporates a composite curve that includes an epicycloid-involute-hypocycloid gear tooth. The tensions in the intersecting helical gear teeth were decreased by raising the angle normal pressure values. The improvement percentages in contact stress and the tooth fillet area were approximately 29.345% and 15.421%, respectively. The most significant improvement in the gear system is attributed to the epicycloid-involute-hypocycloid gear tooth profile. The deviation in the line of action in intersecting helical gears is influenced by slight crossing angles. Kadhim and Abdullah [11] analyzed the effect of tool parameters on the resulting helical gear that integrates involute with epi-hypo-cycloidal profiles. They also assessed the impact of tooth thickness on the gear model, which was generated using the shaper-cutting technique, utilizing a suitable rack-cutter within a Cartesian coordinate framework. The findings indicate that the utilization of a hybrid profile, such as epi, involute, and hypocycloidal, within a single tooth results in an increased area of contact,

thereby enhancing the gears' capacity to endure elevated pressures and extend their operating longevity. The higher stress in the contact area and the cumulative stress in the teeth region improved by approximately 33.169% and 26.08%, respectively, in comparison to the conventional involute profile, and by about 17.69% and 0.67%, respectively, in comparison to the conventional cycloidal profile. Zheng et al. [12] developed a theoretical system to reconfigure mesh excitation waveforms, reducing vibration intensities flexibly across various operating speeds and loads. An improved analytical mesh excitation model accurately determines the load correlation between tip relief and excitation harmonics. A method for tip relief design was proposed that consequently integrates harmonic components of mesh excitations to align with target operating speeds. Comparisons between finite element models and experimental results confirmed the accuracy of both quasi-static and dynamic analyses. The feasibility and effectiveness of the proposed method were demonstrated through parametric studies and application examples.

The current study diverges from prior studies by comparing the present teeth design to a regular gear tooth under identical conditions and by analyzing the unique tooth profile to assess the contact stress area and dynamic performance through two mechanical adjustments. A specialized method has been developed, which may serve as a template for computer numerical control machining to produce a modified crossed helical gear. This study introduces and assesses new strategies for mitigating contact and root stress in crossed helical gear drives, considering anticipated changes in the performance requirements related to drive strength. Surface degradation is a common issue associated with crossed-axes helical gears, which show increased vulnerability to pitting damage. This phenomenon is characterized by the formation of pits that compromise the tooth surface and, in some cases, result in premature tooth failure due to overheating that occurs between the tooth profiles during engagement. Scoring can occur rapidly in high-temperature environments, resulting in an accelerated wear rate. The methods employed to circumvent the scoring region involve the selection of appropriate tooth parameters and the regulation of lubricant flow. This failure is indicated by the presence of pits that progressively enlarge, compromising the tooth surface and, in certain instances, leading to premature tooth fracture [13], [14]. One of the assessments used to evaluate tooth strength is derived from the magnitude of Stress due to Hertzian interaction and the number of stress cycles. Hertzian stress is associated with classical contact mechanics and the deformation of two elastic bodies in contact with one another at one or more points [15]. The contact stress is one of the sources of surface distortion in the non-parallel helical gear system [16]. This investigation determines the angular positions of points that establish surface contact along the arc of action for three contact points between a pair of crossed helical teeth. Standard helical gears and non-standard helical gears are generated utilizing the shaping process. The creation of hybrid teeth gears using a modified gear cutter is a common practice in the industry [17], [18]. Two modifications have been implemented to reduce contact stress and enhance tooth deflection and root stress: 1) tip relief, and 2) compound profile design, which combines involute and epicycloid profiles to prevent the helical gear failure within the gearbox [19]. A comparative analysis was carried out with the three contact point options on the tooth profile to identify the best profile for the crossed helical gear drive.

2. GEOMETRY MODIFICATIONS

Conventional methods are employed to improve transmission error and contact stress between meshing gear teeth. These improvements are achieved through two geometry modifications, which are as follows.

2.1 Tip Relief

The carrying out of tip relief modification mitigates the manufacturing error effect inaccuracies on errors of transmission and stress of contact across different accuracy grades. Tip relief refers to the tooth surface alteration at the tip region that deviates from the traditional involute curve, achieved by the removal of a small quantity of material from it. This modification is employed to prevent early mating between engaging teeth, which can occur due to the deformation of the teeth's profile at an elastic boundary. Tip relief for cylindrical gears with involute surfaces can be quantified by specifying the tip relief amount from the outer circle (radius of addendum, $\boldsymbol{r_a}$), the tip relief form (either intermediate line or parabolic curve), and the point starting on the tooth surface. Three methods can be proposed to define the starting point: (1) the tip relief length, $\boldsymbol{\ell}$ (2) the length of rolling, $\boldsymbol{r_\ell}$, and (3) the angle of rolling, $\boldsymbol{\varphi_\epsilon}$. In Figure 1, it can be seen how the rolling length is related to the rolling angle [20], [21]:

$$r_\ell = r_b\ \varphi_\epsilon \tag{2}$$

where $\boldsymbol{r_b}$ is the radius of the involute base.

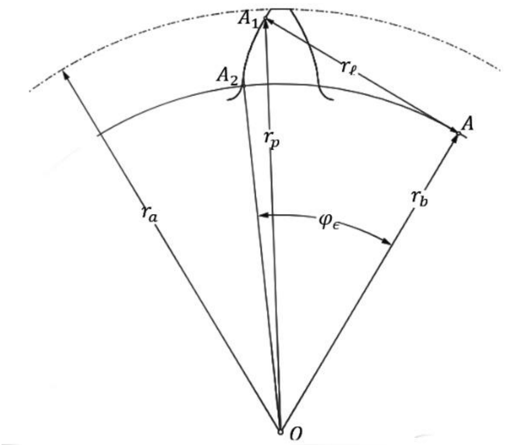

Figure 1. The involutometry relation for length and angle based on rolling

Three types of tip relief can be classified depending on the first location of the tooth tip relief: short, intermediate, and long tip relief. In this study, an intermediate tip relief modification was applied by removing an appropriate amount of material from the gear tooth flank. This adjustment is based on the deformation amount of the tooth within the elastic boundary, which must be removed to correct the transmission error [22]. An essential component in identifying the first point of tip relief is the gear's pitch circle, as outlined below:

$$\ell = r_a - r_p \tag{3}$$

$$r_\ell = \sqrt{{r_p}^2 - {r_b}^2} \tag{4}$$

$$\varphi_\epsilon = \sqrt{\frac{{r_p}^2}{{r_b}^2} - 1} \tag{5}$$

The initial point for tooth tip relief is modified based on the pitch radius, $\boldsymbol{r_p}$ and the addendum radius, $\boldsymbol{r_a}$ of the involute tooth surface. Figure 2 illustrates the topographical shapes (linear and parabolic) for the tooth's tip relief. Figure 3 depicts the relationship between the tip relief length, $\boldsymbol{\ell}$ and the quantity of material removed adjacent to the tooth tip, $\boldsymbol{msl}$. The parameters for the removal of a significant amount and length of relief can be modified based on the elastic tooth deformation required to correct transmission errors. The relief modification at the tooth tip mitigates contact stress and facilitates the smooth engagement of the gear teeth pair, thus reducing the sudden impact between the crossed helical gear teeth [23]. The quantity of materials that can be removed is quantified in terms of roll distance as follows:

$$msl = \frac{F_t}{Fc_s cos\alpha_t} \tag{6}$$

$$\ell = \frac{\overline{AB} - p_{b_t}}{2 - \frac{{F^{(12,n)}}_{design}}{c_s\, msl\, F\, cos\alpha_t}} \tag{7}$$

$\boldsymbol{F_t}$: Tangential force

$\boldsymbol{F}$: Face width

$\boldsymbol{c_s}$: Tooth mesh stiffness

$\boldsymbol{\alpha_t}$: Transverse pressure angle

$\overline{\boldsymbol{AB}}$: Tooth distance

$\boldsymbol{p_{b_t}}$: Base pitch

In this study, MATLAB was used to estimate the transmission error [24]. The program was conceived in accordance with the principles of gearing theory. The calculations consist of five rows and twenty-five columns, where the rows correspond to the lines of contact and the columns represent slices that cross the helical teeth width. The input parameters for the matrices included microparameters, such as tip relief and helix relief. Furthermore, interferences between gear surfaces were incorporated to assess the interference at certain spots along the contact lines [25].

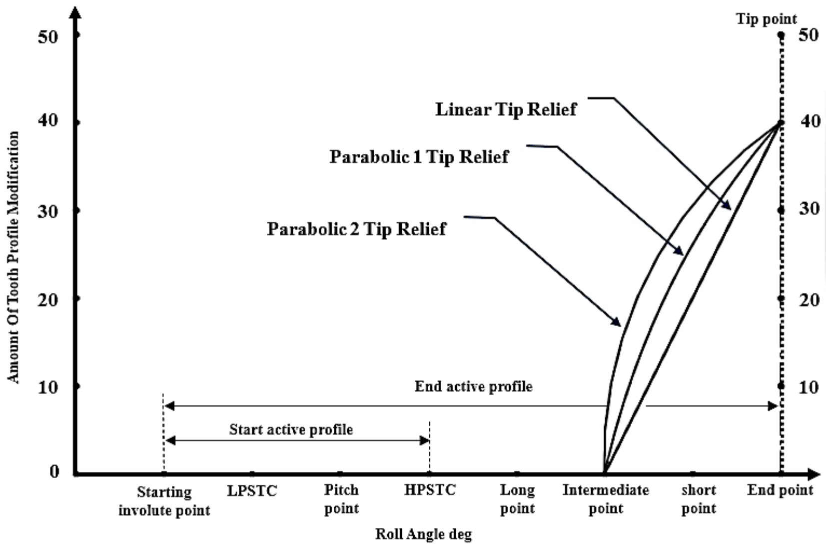

Figure 2. The topographical tooth's tip relief shape

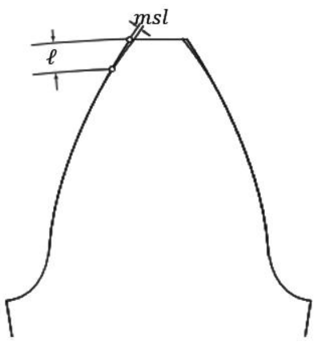

Figure 3. The relationship between the tip relief length and the amount of relief

2.2 Modified Involute or Compound Tooth System

This work features the second mechanical modification, which is the integration of an involute surface with an epicycloid surface. The integrated tooth surface is engineered to reduce deflection of the teeth, as well as bending and contact stresses, thereby mitigating the risk of failure in the gearbox's pinion. The proposed crossed helical gear features an involute-epicycloid conjugate profile. The structure comprises an involute section adjacent to the pitch area and an epicycloid tooth profile extending to the addendum circle. The convex flank of one cycloidal tooth engages with the concave flank of the corresponding tooth, resulting in an extensive contact area that enhances wear resistance. The contact in the involute gear profile occurs between two convex surfaces on the meshing teeth, leading to a reduced contact area and diminished wear resistance. Figure 4 illustrates a cross-section of the profile of a composite tooth, which consists of an involute-epicycloid curve [26], [27].

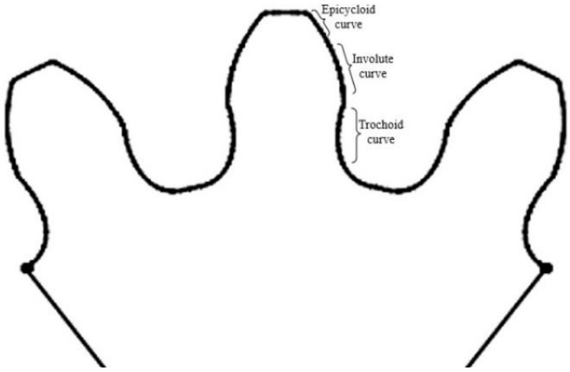

Figure 4. The cross-section of the compound tooth profile

The trajectory of a point that is closely associated with a circle and rolls over another circle is the basis for epicycloid curves, as shown in Figure 5. γ_1 and γ_2 are the radii of the cycloid circles' creation. Point M is firmly attached to the second gear's circle and draws out an epicycloid, which is firmly linked to the circle of the first gear within the original coordinates system [28].

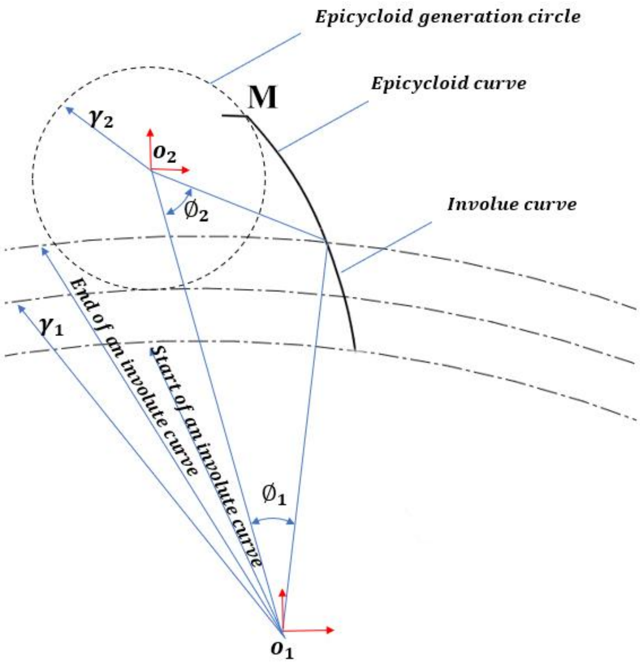

Figure 5. Epicycloid curves

Epicycloid curves are yielded by the following equations:

$$x = (\gamma_1 + \gamma_2) sin\emptyset_1 - a\ sin\left[\emptyset_2\left(1 + \frac{\gamma_1}{\gamma_2}\right)\right] \quad (8)$$

$$y = (\gamma_1 + \gamma_2) cos\emptyset_1 - a\ cos\left[\emptyset_2\left(1 + \frac{\gamma_1}{\gamma_2}\right)\right] \quad (9)$$

where $a = O_2M > \gamma_2$

In practice, involute tooth systems are employed in industry due to their ease of manufacturing and cost-effectiveness. The involute curve extends from the inner circle and toward the outer circle, and one pair of tooth surfaces is in contact with a small fraction of another surface. The creation of an involute curve is done at a point fixed by a straight line that rolls without slipping over a generating circle of toothed gears. The following equations provide the basis for the involute curve derivation. [29]:

$$x = -a sin\emptyset + R_b(sin\emptyset - \emptyset cos\emptyset) \tag{10}$$

$$y = -a cos\emptyset + R_b(cos\emptyset + \emptyset sin\emptyset) \tag{11}$$

One issue with the involute profile is interference. The motion is not transmitted continuously; rather, a subsequent pair of teeth must engage before disengaging the first pair. There is invariably a period of simultaneous overlap between two pairs of meshed teeth. The configuration of the tooth surface, the teeth number, and the positioning of the gear pair during meshing contribute to the interference between the flanks of the gear teeth [30]. It is essential to identify a strategy for mitigating or eliminating this interference. The objective is to reposition the working profiles along the involute curve to exclude the segment near the gear teeth base, thus enhancing the contact conditions for the tooth surfaces [31]. The analytical method to avoid the undesired area of the teeth is by cutting the common tangent to the base circles between the points of tangency. The defining condition will be satisfied when the outer circles of the driver and driven gear pass through points C_1 and C_2, respectively, as illustrated in Figure 6.

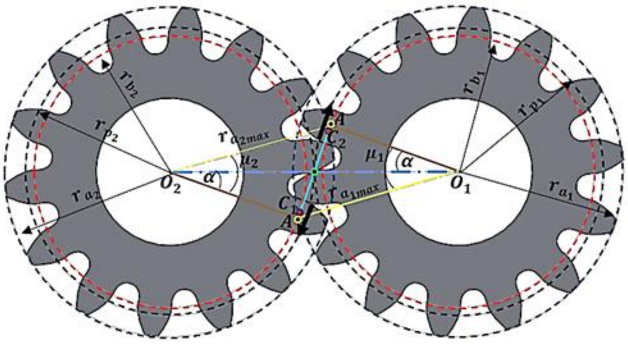

Figure 6. Gear tooth engagement

In order to prevent interference, the maximum allowable radius between the pinion and the tip of the gear teeth has been determined. The following equations, derived from research, are essential for determining the largest feasible radius:

ΔO_1PA

$$(O_1A)^2 = (O_1P)^2 + (PA)^2 - 2(O_1P)(PA)cos\,(ang(O_1PA)) \tag{12}$$

$$(r_{a_{1max}})^2 = (r_{p_1})^2 + (r_{p_2}\,sin(\alpha))^2 - 2r_{p_1}r_{p_2}sin\,(\alpha)cos\,(90+\alpha) \tag{13}$$

$$(r_{a_{1max}})^2 = (r_{p_1})^2 + (r_{p_2}\,sin(\alpha))^2 + 2r_{p_1}r_{p_2}sin\,(\alpha)sin\,(\alpha) \tag{14}$$

$$(r_{a_{1max}})^2 = (r_{p_1})^2 + (r_{p_2}\,sin(\alpha))^2 + 2r_{p_1}r_{p_2}(sin\,(\alpha))^2 \tag{15}$$

$$(r_{a_{1max}})^2 = (r_{p_1})^2\left[1 + \frac{(r_{p_2}\,sin(\alpha))^2}{(r_{p_1})^2} + \frac{2r_{p_1}r_{p_2}(sin\,(\alpha))^2}{(r_{p_1})^2}\right] \tag{16}$$

$$(r_{a_{1max}})^2 = (r_{p_1})^2\left[1 + \frac{r_{p_2}}{r_{p_1}}\left(\frac{r_{p_2}}{r_{p_1}} + 2\right)(sin\,(\alpha))^2\right] \tag{17}$$

$$r_{a_{1max}} = r_{p_1}\sqrt{1 + \frac{r_{p_2}}{r_{p_1}}\left(\frac{r_{p_2}}{r_{p_1}} + 2\right)(sin\,(\alpha))^2} \tag{18}$$

$$r_{a_{2max}} = r_{p_2}\sqrt{1 + \frac{r_{p_1}}{r_{p_2}}\left(\frac{r_{p_1}}{r_{p_2}} + 2\right)(sin\,(\alpha))^2} \tag{19}$$

The maximum possible radius on the pinion to avoid interference, = (O_1A) — (O_1P) = r.

$$r = r_{p_2}\sqrt{1 + \frac{r_{p_1}}{r_{p_2}}\left(\frac{r_{p_1}}{r_{p_2}} + 2\right)(sin\,(\alpha))^2} - r_{p_1} \tag{20}$$

The maximum radius parameter is used to determine the start position of the involute-epicycloid curve on the rolling circle.

3. GENERATION OF HELICAL GEAR TEETH BY CUTTER TOOLS

In this analysis, three types of helical gear drives were generated for comparison purposes. The standard helical gear, along with two modifications of helical gear drives, were produced using a rack-cutter, which is a common practice in the industry. The process of generating these gears using a rack-cutter is illustrated in Figure 7. The cutting-blank cylinder spins at an angle to the rotational axis alongside the rack-cutter, which moves quickly along the centroidal line. The linear velocity and rotational velocity are expressed as follows:

$$\frac{v}{w} = r_p = \frac{Z}{D_p} \tag{21}$$

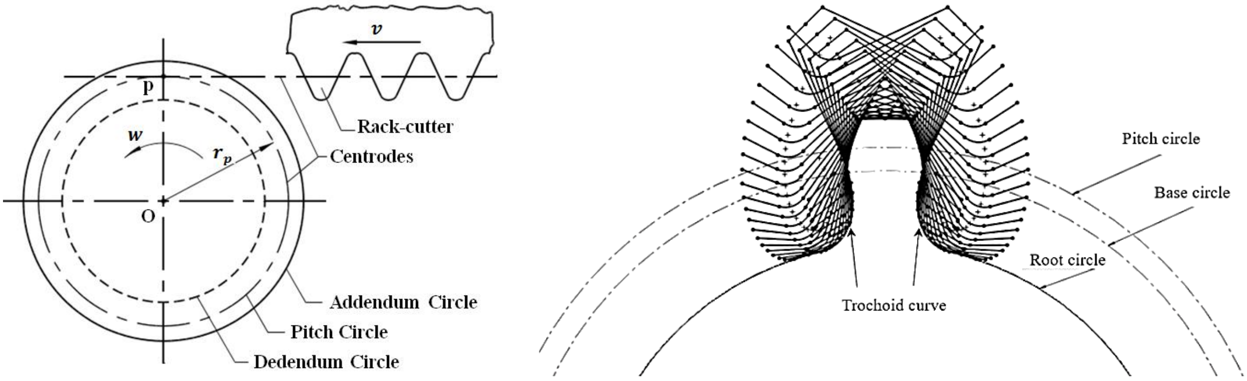

Figure 7. Generation of the tooth profile using a rack-cutter

The circle of pitch is an imaginary gear circle. It is a gear centrode by cutting. The cutting tool center is the horizontal line that is tangent to the operating circle and may be parallel to the linear velocity of the rack. Throughout the cutting operation, the rack-cutter rotates in a circular motion that is perpendicular to the gear axis. The cross-section of the resulting tooth shape is created by a set of various rack positions that are sequenced in a logical order to form the whole tooth. The final shape is represented by the coordinate system rigidly connected to the gear being created. The shape of the tooth is a conventional involute curve [32], [33]. This curve is characterized by a base circle denoted as r_b and it is determined as follows:

$$r_b = \frac{Z\, cos\alpha}{2D_p} \tag{22}$$

$$r_b = r_p cos\alpha \tag{23}$$

or:

$$r_b = \frac{v}{w} cos\alpha \tag{24}$$

where α is the angle of the rack-cutter or the normal pressure angle of the gear tooth profile.

The principles of the computer program are established through the application of gear tooth envelope theory. Various curves of the tooth surface can be produced using a non-standard rack-cutter. The computer program was developed using the QBasic language. The resulting shape was imported into the SolidWorks software. The application programming interface was utilized to simulate the generation of gear teeth. The primary approach of generation through coordinate transformation was utilized in deriving curves and surfaces that represent the gear tooth profile. The method of coordinate transformation is used in deriving the equation for the helicoid surface, which is formed as a family of curves of identical shape. [22].

4. ANALYSIS OF CROSSED HELICAL GEARS MODELING

Figure 8 depicts the fundamental study of the connecting topology of crossed helical gear drives. The surface of the tooth profile geometry is generated by helical involute gears. The rotation axes of two intersecting helical gears intersect at the crossing angle λ. The minimal distance between the gears is E. The pitch cylinders make contact at a single point P, referred to as the pitch point. The angle of the helix at their pitch cylinder is denoted as β_p, while those at their base cylinders are represented as β_b. The angles of rotation for both gears are θ_1 and θ_2. The normal modulus is denoted as m_n, the transverse modulus is represented as m_t, and the angles of pressure in the normal plane section and the transverse plane section are α_n and α_t, respectively. The teeth number is indicated as Z. The global coordinate system is defined by the axes x, y, and z. Correspondingly, x_1, y_1, and z_1 and x_2, y_2, and z_2 depict the systems of model coordinates for gear 1 and gear 2, respectively, and are defined in relation to the global system. The y_1 and y_2 axes correspond to the rotation axes of gear 1 and gear 2, respectively. The remaining axes complete the coordinate system for the two gears [34].

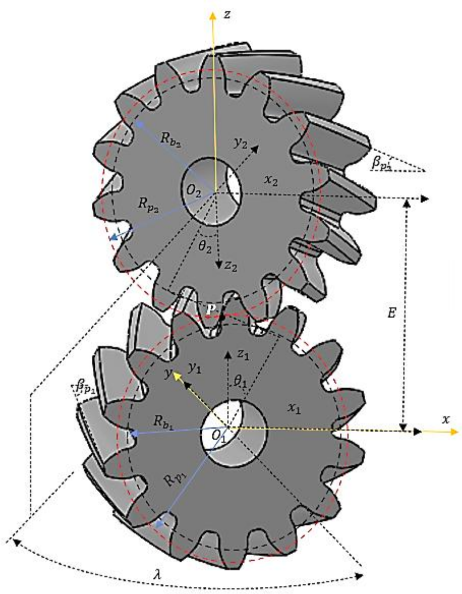

Figure 8. Geometry of non-parallel helical gears at a crossing angle of 45°

The pitch points are determined according to Figure 8. Let $p_1(x_{p_1}, y_{p_1}, z_{p_1})$ represent the system of model coordinates of the pitch point for gear 1. The coordinate system of the pitch point for gear 2 is represented as $p_2(x_{p_2}, y_{p_2}, z_{p_2})$. These coordinate systems are required to facilitate the calculations.

$$z_{p_1} = E - \frac{r_{p_1}}{cos\theta_1} \tag{25}$$

$$z_{p_2} = \frac{r_{p_2}}{cos\theta_2} \tag{26}$$

$$y_{p_2} = 0 \tag{27}$$

$$x_{p_{2-2}} = 0 \tag{28}$$

$$x_{p_{1-2}} = \frac{E - \frac{r_{p_1}}{cos\theta_1} - \frac{r_{p_2}}{cos\theta_2}}{-sin\theta_2\, cos\beta_{b_2}} \times \left(-cos\theta_2\, cos\beta_{b_2}\right) \tag{29}$$

$$y_{p_2} = \frac{\frac{r_{p_2}}{cos\theta_2} - E - \frac{r_{p_1}}{cos\theta_1}}{sin\theta_1\, cos\beta_{b_1}} \times \left(cos\theta_1\, cos\beta_{b_1}\right) \tag{30}$$

$$y_{p_{1-2}} = \frac{-sin\lambda}{cos\lambda} \times \frac{E - \frac{r_{p_1}}{cos\theta_1} - \frac{r_{p_2}}{cos\theta_2}}{-sin\theta_2\, cos\beta_{b_2}} \times \left(-cos\theta_2\, cos\beta_{b_2}\right) \tag{31}$$

$$y_{p_{2-2}} = \frac{\frac{\frac{r_{p_2}}{cos\theta_2} - E - \frac{r_{p_1}}{cos\theta_1}}{sin\theta_1\, cos\beta_{b_1}} \times \left(cos\theta_1\, cos\beta_{b_1}\right)}{cos\lambda} \tag{32}$$

$$\begin{aligned} x_{p_1} = {} & \frac{E - \frac{r_{p_1}}{cos\theta_1} - \frac{r_{p_2}}{cos\theta_2}}{-sin\theta_2\, cos\beta_{b_2}} \times \left(-cos\theta_2\, cos\beta_{b_2}\right) \times cos\lambda — sin\lambda cos\lambda \times \frac{E - \frac{r_{p_1}}{cos\theta_1} - \frac{r_{p_2}}{cos\theta_2}}{-sin\theta_2\, cos\beta_{b_2}} \\ & \times \left(-cos\theta_2\, cos\beta_{b_2}\right) \times sin\lambda \end{aligned} \tag{33}$$

$$\begin{aligned} y_{p_1} = {} & \frac{E - \frac{r_{p_1}}{cos\theta_1} - \frac{r_{p_2}}{cos\theta_2}}{-sin\theta_2\, cos\beta_{b_2}} \times \left(-cos\theta_2\, cos\beta_{b_2}\right) \times sin\lambda \\ & + \frac{-sin\lambda}{cos\lambda} \times \frac{E - \frac{r_{p_1}}{cos\theta_1} - \frac{r_{p_2}}{cos\theta_2}}{-sin\theta_2\, cos\beta_{b_2}} \times \left(-cos\theta_2\, cos\beta_{b_2}\right) \times cos\lambda \end{aligned} \tag{34}$$

$$x_{p_2} = -\frac{\dfrac{\dfrac{r_{p_2}}{cos\theta_2} - E - \dfrac{r_{p_1}}{cos\theta_1}}{sin\theta_1\ cos\beta_{b_1}} \times \left(cos\theta_1\ cos\beta_{b_1}\right)}{cos\lambda} \times sin\lambda \tag{35}$$

$$y_{p_2} = \frac{\dfrac{\dfrac{r_{p_2}}{cos\theta_2} - E - \dfrac{r_{p_1}}{cos\theta_1}}{sin\theta_1\ cos\beta_{b_1}} \times \left(cos\theta_1\ cos\beta_{b_1}\right)}{cos\lambda} \times cos\lambda \tag{36}$$

To determine the pitch points positions p_1 and p_2 in the notation for vectors:

$$\overrightarrow{p_1} = \begin{bmatrix} x_{p_1} \\ y_{p_1} \\ z_{p_1} \end{bmatrix} = \begin{bmatrix} cos\lambda \times x_{p_{1-2}} - sin\lambda \times y_{p_{1-2}} \\ sin\lambda \times x_{p_{1-2}} + cos\lambda \times y_{p_{1-2}} \\ E - \dfrac{r_{p_1}}{cos\theta_1} \end{bmatrix} \tag{37}$$

$$\overrightarrow{p_2} = \begin{bmatrix} x_{p_2} \\ y_{p_2} \\ z_{p_2} \end{bmatrix} = \begin{bmatrix} -sin\lambda \times \dfrac{\dfrac{\dfrac{r_{p_2}}{cos\theta_2} - E - \dfrac{r_{p_1}}{cos\theta_1}}{sin\theta_1\ cos\beta_{b_1}} \times \left(cos\theta_1\ cos\beta_{b_1}\right)}{cos\lambda} \\ cos\lambda \times \dfrac{\dfrac{\dfrac{r_{p_2}}{cos\theta_2} - E - \dfrac{r_{p_1}}{cos\theta_1}}{sin\theta_1\ cos\beta_{b_1}} \times \left(cos\theta_1\ cos\beta_{b_1}\right)}{cos\lambda} \\ \dfrac{r_{p_2}}{cos\theta_2} \end{bmatrix} \tag{38}$$

In this case, the operating cylinders are moving along the x-axis. Through this location, the action line passes through this point. Figure 9 displays the cross-sectional view of the pitch cylinders' angular velocities w_1 and w_2 at an angle λ.

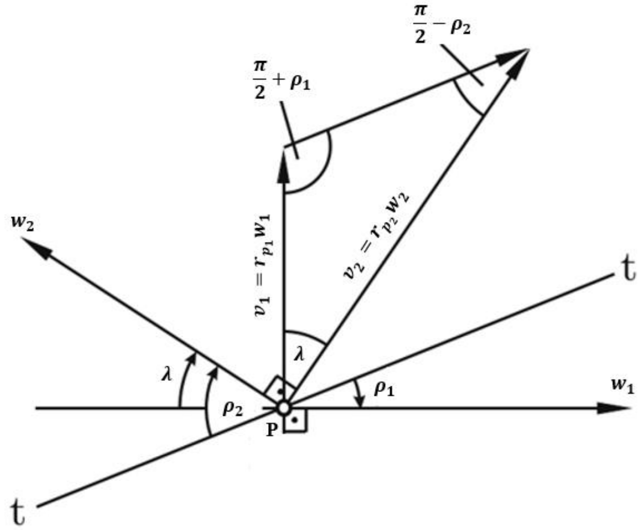

Figure 9. The polygon of angular velocities

A common normal line $\overline{tt}$ that passes through a fixed point associated with the point of contact bisects the central distance intersecting at the pitch point. As in this figure, the axis $\overline{tt}$ forms an angle ρ_i with the horizontal gear axis $(i = 1, 2)$. In the original position at point p, the pitch velocities for crossed helical gears were resolved into two components v_1 and v_2 have directions as shown in Figure 9 and magnitude values $r_i w_i$ $(i = 1, 2)$. The relative velocity of sliding $|v_2 - v_1|$ is a parallel direction with the straight $\overline{tt}$. Furthermore, utilizing the sine rule in relation to the velocity polygon, encompassing the angles, λ, $\pi / 2 + \rho_1$, and $\pi / 2 + \rho_2$, results indicate that the angular velocity is constant and is demonstrated by the relationship $(r_2 w_2)/(\cos\rho_1) = (r_1 w_1)/(\cos\rho_2)$. As for the sliding velocity $|v_2 - v_1|$, the cosine law produces the following formula. [35]:

$$|v_2 - v_1| = w_1 r_1 \sqrt{1 + (\frac{w_2 r_2}{w_1 r_1})^2 - 2\frac{w_2 r_2}{w_1 r_1} cos\ (\lambda)} \tag{39}$$

Synchronously, the engagement between the helical teeth, the tooth begins rolling from the starting contact point at the tooth's tip for pinion in the tooth's root area for gear and ends at the point with the contact of the tooth's tip of pinion in the tooth's root area of gear. The coordinates of both the starting and ending points were determined based on the surface angles at the outer diameter required for gears as follows:

$$\gamma_i = cos^{-1}\frac{r_{b_i}}{r_{a_i}} \quad (i = 1,2) \tag{40}$$

$$\alpha = cos^{-1}\frac{r_{b_i}}{r_{p_i}} \quad (i = 1,2) \tag{41}$$

The contact line $\overline{AA}$ situated on the contact line is restricted to the section $\overline{C_1C_2}$ within the outer circles with radii r_{a_1} and r_{a_2}. They are defined by the angles μ_1 and μ_2. The length of the segment line ȴ can be determined using the following calculation:

$$ȴ_i = r_{b_i}(tan\mu_i - tan\alpha) \qquad (i = 1,2) \tag{42}$$

The distance between the engagement sites of consecutive teeth is:

$$\delta = \frac{2\pi r_{b_i}}{Z_i} \tag{43}$$

Here, $\boldsymbol{\delta}$ is the length of the arc. The contact ratio equals to:

$$C_r = \frac{ȴ}{\delta} \tag{44}$$

The formula for the contact ratio of skewed helical gear axes is [35]:

$$C_r = \frac{1}{2\pi}\left\{Z_1\left(\frac{tan\mu_1 - \frac{tan\alpha}{cos\beta_{p_1}}}{cos^2\beta_{p_1}}\right) + Z_2\left(\frac{tan\mu_2 - \frac{tan\alpha}{cos\beta_{p_2}}}{cos^2\beta_{p_2}}\right)\right\} \tag{45}$$

5. GENERAL CONSIDERATIONS

It is evident that the cross-based cylinders of the helical gears, as depicted in Figure 10, possess a common tangent line. Two lines, $\overline{A_1}$ and $\overline{A_2}$, are tangent to the base cylinders at points A_{11}, A_{12}, A_{21}, and A_{22}. The lines conform to the meshing of the appropriate flanks of the tooth profiles and intersect at point P. Figure 11 shows the relationship between the base cylinders and the action lines for a system of two crossed helical gears that make contact at point P.

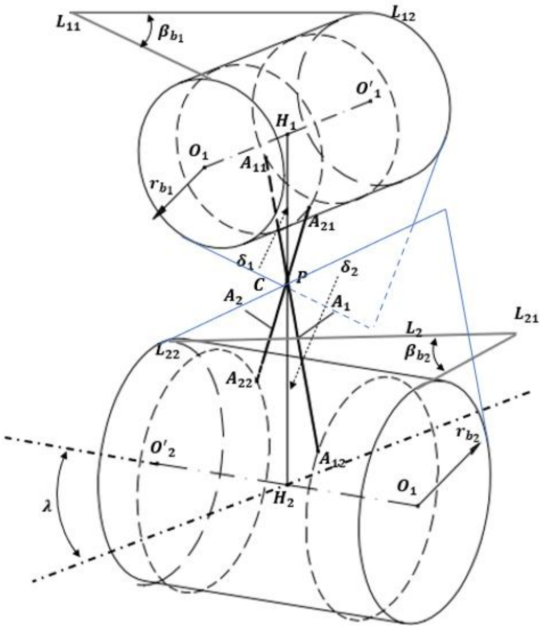

Figure 10. Relationship between the lines of action and the axis of rotation

The crossing angle between the axes of rotation is $\boldsymbol{\lambda}$, while β_{b_1} and β_{b_2} are angles base helix. The line $\overline{H_1H_2}$ is a common tangent to two centerlines of both cylinders and passes through the contact point. The contacting point C moves on the course of action in the normal section. Curvature radii of the two teeth's surfaces are δ_1 and δ_2. Curvature radii at the pitch point are defined by δ_{1p} and δ_{2p}, which are expressed by the following equations [36]:

$$\delta_{1p} = \frac{r_{p_1}sin\alpha_n}{cos^2\beta_{b_1}} \tag{46}$$

$$\delta_{2p} = \frac{r_{p_2} sin\alpha_n}{cos^2\beta_{b_2}} \tag{47}$$

The radii of curvatures δ_1 and δ_2 for tooth surfaces are independent of the position of the contact point C. The length of the course of action ɥ is calculated as follows [37]:

$$ɥ = \frac{E - r_{b_1} cos\alpha_{t_1} - r_{b_2} cos\alpha_{t_2}}{sin\alpha_n} = \frac{r_{b_1}\, tan\alpha_{t_1}}{cos\beta_{b_1}} + \frac{r_{b_2}\, tan\alpha_{t_2}}{cos\beta_{b_2}} \tag{48}$$

$$ɥ = \delta_1 + \delta_2 = \delta_{1p} + \delta_{2p} \tag{49}$$

$$ɥ = \delta_{1max} + \delta_{2min} = \delta_{1min} + \delta_{2max} \tag{50}$$

The radius of equivalent cylinders is represented by:

$$\delta_{1max} = \frac{\sqrt{r_{a_1}^2 - r_{b_1}^2}}{cos\beta_{b_1}} \tag{51}$$

$$\delta_{2min} = \frac{\sqrt{r_{a_2}^2 - r_{b_2}^2}}{cos\beta_{b_2}} \tag{52}$$

$$\delta_{1min} = ɥ - \delta_{2min} \tag{53}$$

$$\delta_{2max} = ɥ - \delta_{1max} \tag{54}$$

Figure 11 shows the engagement of the crossed axes of the helical gear and the relationship between the enclosed angles Ω_1, Ω_2, and ϑ. These relationships are represented in the figure and are described by the following equations:

$$\Omega_1 = tan^{-1}\left(tan\beta_{p_1}\, sin\alpha_n\right) \tag{55}$$

$$\Omega_2 = tan^{-1}\left(tan\beta_{p_2}\, sin\alpha_n\right) \tag{56}$$

$$\vartheta = \Omega_1 + \Omega_2 \tag{57}$$

Therefore, the relationship between the angle enclosed by two contact lines and the crossing angle is:

$$\vartheta = \sin^{-1}\left(\frac{\sin\alpha_n \sin\lambda}{\cos\Omega_1 \cos\Omega_1}\right) \tag{58}$$

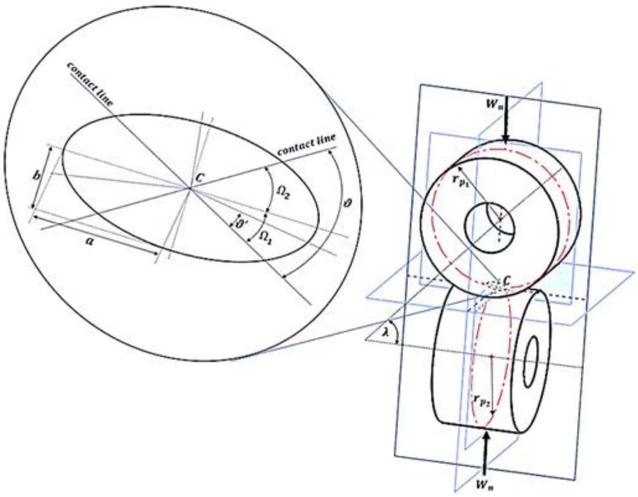

Figure 11. Engagement of a crossed-axes helical gear

5.1 Contact Ellipse

The engagement of the gear tooth surfaces in a crossed helical gear drive can be represented by the contact between two equivalent cylinders skewed under an angle ϑ. The geometrical contact between these two cylinders occurs at point C. Due to the elastic boundary of gears, the point of contact changes into an instantaneous contact ellipse, wherein the contacting point is distributed over an elliptical area. Theoretical tangency is at the same location as the contact ellipse center. A series of contact ellipses constitutes the bearing contact. This investigation aims to find the direction of the contact ellipse in the plane tangent to the contacting surfaces. The elastic deformation depends on the applied load. Figure 12 illustrates the normal pressure exerted on the engaged gear tooth surfaces. The contact pressure is distributed over a small area, resulting in the formation of maximum contact stress.

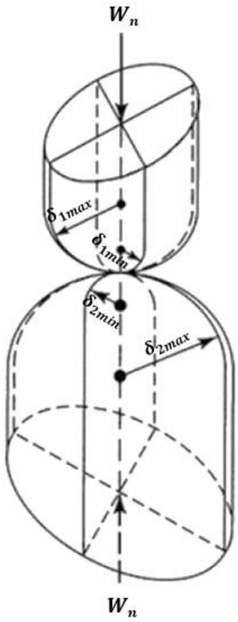

Figure 12. Distribution of stress

Two cylinders, with radii denoted as r_{p_1} and r_{p_2}, are in contact at point *C*. Both axes of rotation are skewed at a crossing angle λ. During the engagement, the normal load W_n is applied, producing a contact ellipse. The lengths of the major and minor axes for the contact ellipse are defined by *2a* and *2b*, respectively. Here, the angle between the two principal planes of radii δ_1 and δ_2 is denoted by ϑ. Meanwhile, the angle between the major axis of the contact ellipse and the principal plane of the radius of curvature δ_1 is denoted by ϑ'. This angle can be calculated as follows [38], [39]:

$$\vartheta' = \frac{1}{2} tan^{-1}\left(\frac{\frac{\delta_1}{\delta_2}\, sin2\vartheta}{1+\frac{\delta_1}{\delta_2}\, cos2\vartheta}\right) \tag{59}$$

5.2 Contact Stress

This work considers the high-intensity value of the stress in contact with other stresses induced in gear teeth as an indicator in the analysis. Gear teeth that are stronger than the material's surface endurance strength reduce the likelihood of surface fatigue failure. Hertz equation was derived and used to calculate the induced contact stress between elastic cylinders under a skewed axis angle. Two methods were used to obtain the complete elliptic integral of the second kind: the numerical approximation method and the arithmetic-geometric mean. These methods are considered precise for calculating complete elliptic integrals. The maximum contact stress was determined by utilizing the Hertzian auxiliary coefficients € and £, which are derived from the complete elliptic integral of the second kind, as referenced in [40], [41], and [42]:

$$€ = \left(\frac{2}{\pi}\,\frac{E(K)}{1-K^2}\right)^{\frac{1}{3}} \tag{60}$$

$$£ = \left((1-K^2)^{\frac{3}{2}}\,\frac{2}{\pi}\,\frac{E(K)}{1-K^2}\right)^{\frac{1}{3}} \tag{61}$$

or

$$£ = (1-K^2)^{\frac{1}{2}}\ € \tag{62}$$

The auxiliary coefficients are used to find two constants, *a* and *b*:

$$a = \left(3\,€^3\,\frac{(1-v^2)\,W_n}{E\sum\frac{1}{\delta}}\right)^{\frac{1}{3}} \tag{63}$$

$$b = \left(3\,£^3 \, \frac{(1 - v^2)\, W_n}{E \sum \frac{1}{\delta}} \right)^{\frac{1}{3}} \tag{64}$$

The following formula calculates the maximum contact stress.

$$W_{max} = \frac{3}{2} \frac{W_n}{\pi\, a\, b} \tag{65}$$

6. RESULTS AND DISCUSSION

6.1 Estimation of Static Transmission Error

MATLAB was used to estimate the static transmission error at each point of contact along the course of action. The mesh cycle was divided into 16 steps. Each step equals one sample of the base pitch or (p_b/16). The face width was divided into 25 slices. The program is based on the following design parameters:

i) Tangential load applied.
ii) Base pitch and base helix angle are specified by the tooth geometry.
iii) The number of misalignments and deflections.
iv) Tooth stiffness.
v) Start of linear relief.
vi) Interference at the pitch area.

The technique is based on the estimated value of transmission error to produce a new applied load value. The comparison between the original and new values was performed continuously until the error percentage converged to an acceptable level. The computation of the mesh cycle for static transmission error was established through the procedure that was repeated at each part of the mesh cycle. The procedure is illustrated in Figure 13. The results indicate that the optimal value of transmission error corresponds to an intermediate tip relief.

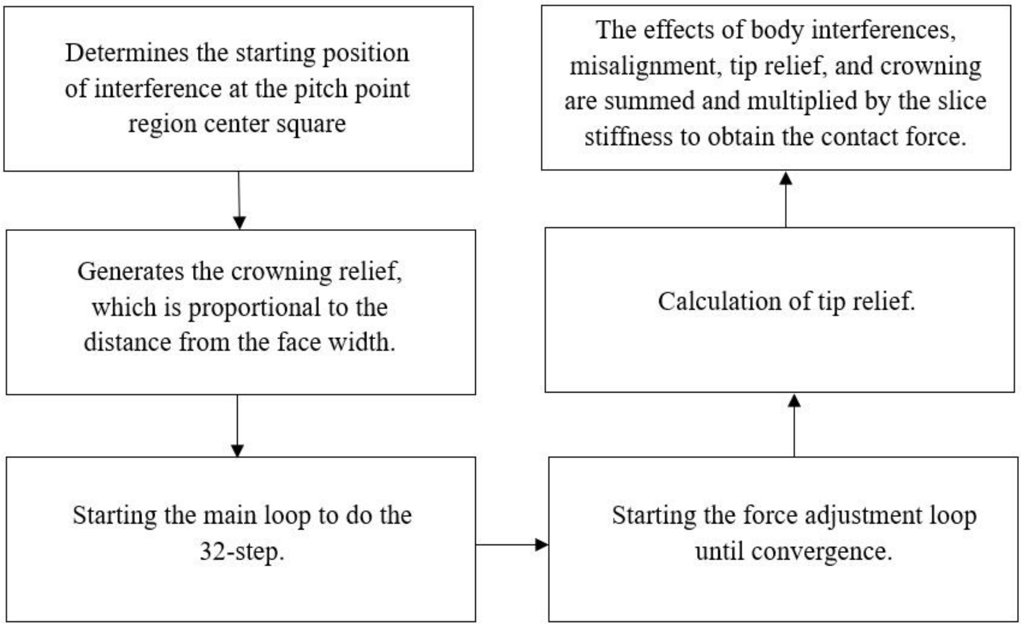

Figure 13. The steps involved in the MATLAB program

The results indicate that, for a contact load design of 20 kN, the average value of deflection resulting from elastic tooth deflection is disregarded, as only the vibrational variations are significant for noise considerations. Figures 14(a), 14(b), 14(c), and 14(d) are similar; however, they differ in the quantity of misalignment values. The error in transmission from peak to peak is also analogous to similar instances of models. The waveform is expected to improve, leading to a reduction in harmonics. Figure 14(e) depicts the anticipated static transmission error for minimal misalignment, with relief commencing at a decreased distance of base pitch from the pitch point to the end. The initiation of the active profile has been advanced significantly along the flank, resulting in a decrease in peak-to-peak transmission error. Furthermore, the waveform exhibits higher harmonics. However, the dynamic characteristics of meshed teeth imply that the applied power not only influences the magnitude of the amplitudes of mesh deformation, as is commonly acknowledged, but also modifies the waveforms of mesh excitation, presenting significant challenges for conventional design to accommodate diverse operating conditions. Figure 15 shows the relationship between the error of transmission and the quantity of tip relief. The variation in the slope of the relationship line signifies that the rectification of the standard manufacturing error, which induces transmission error, increases by removing appropriate quantities of tooth tip material in accordance with the elasticity of tooth deflection and misalignment.

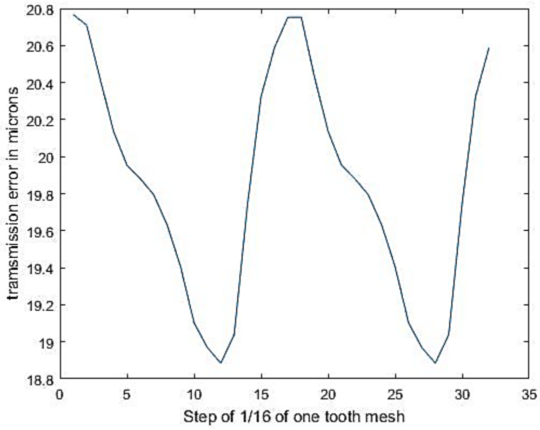

(a) $msl = 30\ \mu m, p_b = 0.0177\ mm$

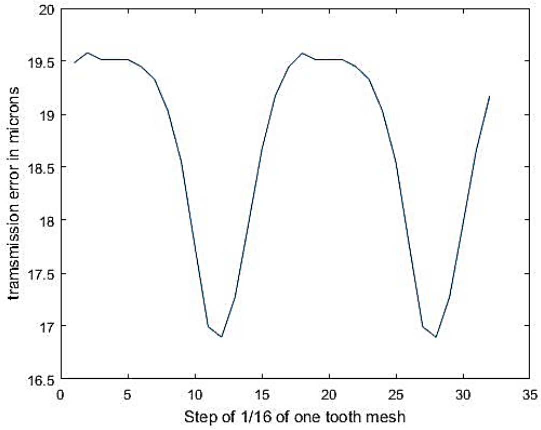

(b) $msl = 40\ \mu m, p_b = 0.0177\ mm$

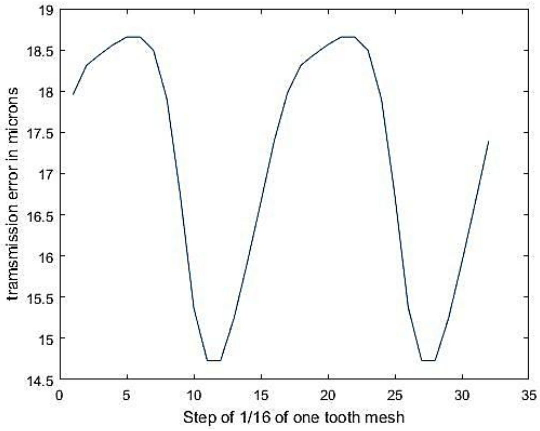

(c) $msl = 50\ \mu m, p_b = 0.0177\ mm$

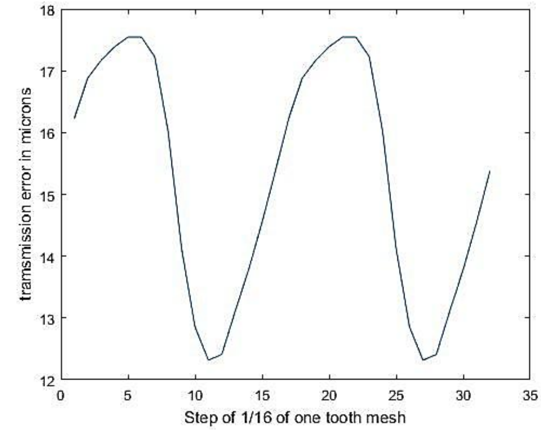

(d) $msl = 60\ \mu m, p_b = 0.0177\ mm$

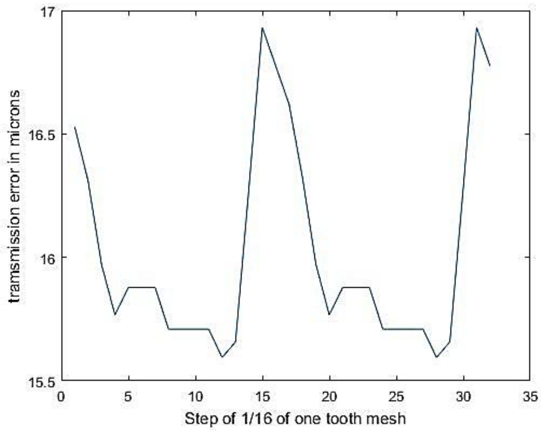

(e) $msl = 60\ \mu m, p_b = 0.4\ mm$

Figure 14. Results of the estimation of static transmission error

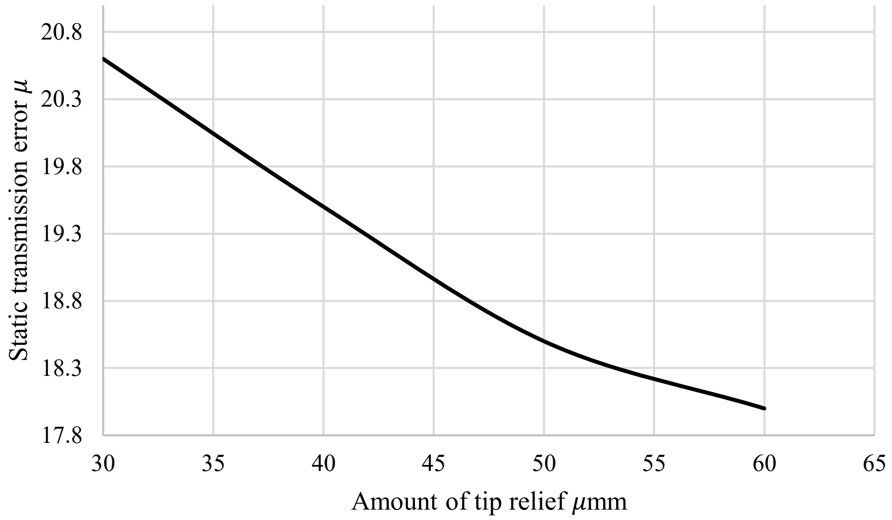

Figure 15. The relationship between the error of transmission and the quantity of tip relief

5.3 Generation of Standard and Non-standard Gear Tooth Profiles

The configuration of the gear tooth is determined according to the form of the cutting tool. Figure 16 depicts the methodologies used to obtain three-dimensional (3D) helical gear profiles. Three rack-cutters were used to fabricate three types of helical gears: a conventional standard cutter, cutter 1, which features tip relief modification, and cutter 2, which incorporates cycloidal modification, as depicted in Figure 17. The input parameters are the gear teeth, angles of pressure and helix, module, and face width, in addition to the length and amount of tip relief. These data can be used to simulate the generation of a fully modified gear. The process begins with the first point at the root fillet of the cutter and progresses sequentially through the points until reaching the relevant points on the gear tooth. The finishing condition is met when the final intersection point on a tooth is located beyond the circle of the addendum.

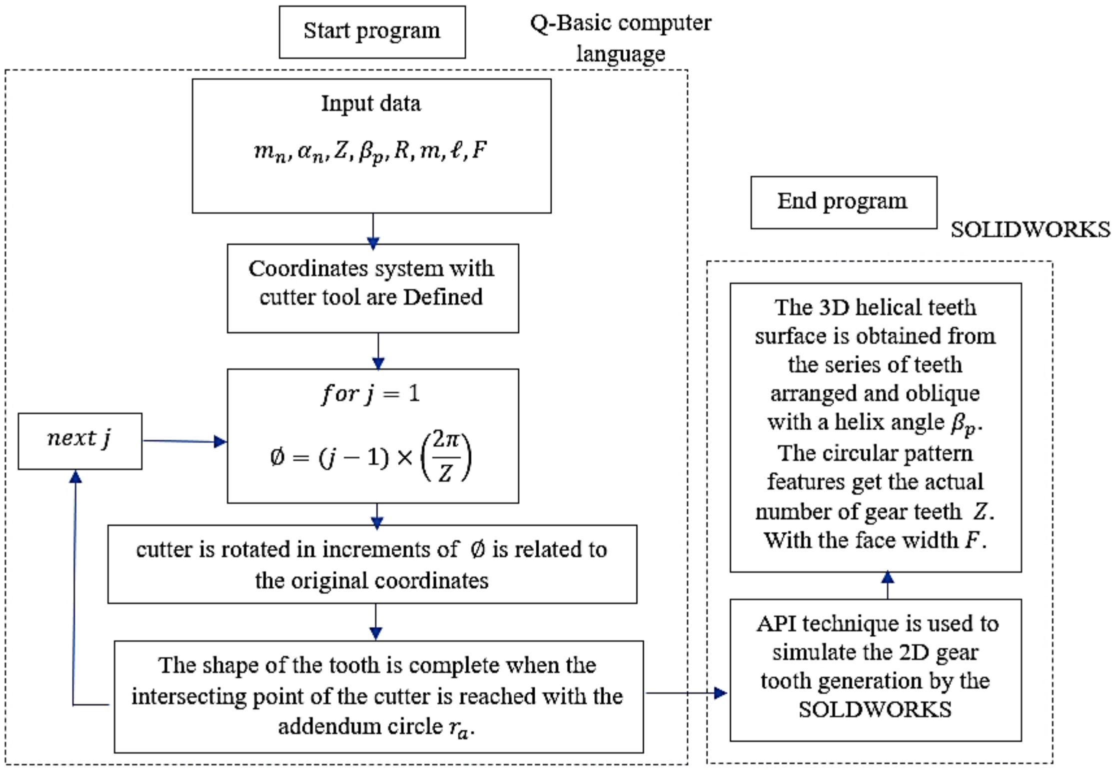

Figure 16. The processes involved in the generation of helical gear teeth

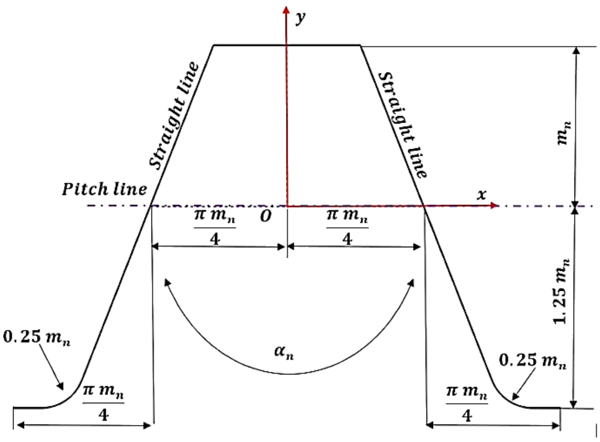

(a) Classic standard cutter

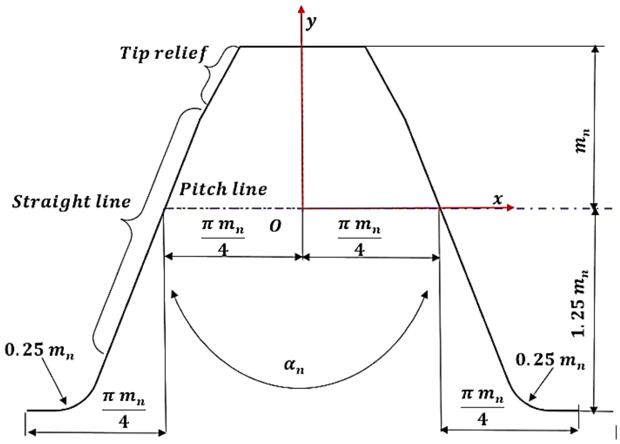

(b) Cutter 1 with tip relief modification

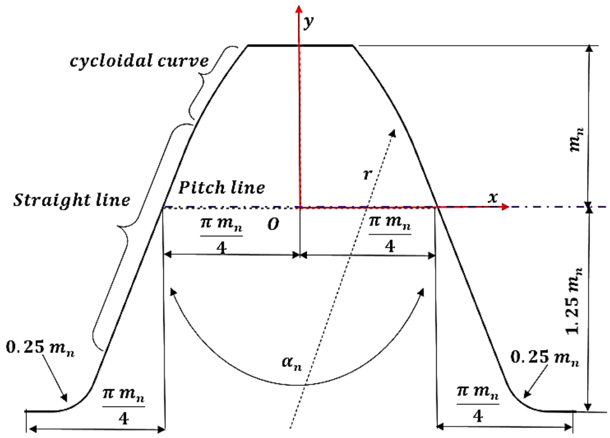

(c) Cutter 2 with cycloidal modification

Figure 17. Coordinate system of cutter tools

Three two-dimensional (2D) gear tooth profiles were developed using the QBasic programming language. A computer application was designed to simulate rack-cutting tools. The creation process involves the rolling motion of the cutter's right and left sides. The starting position is at the origin (pitch point), followed by positive and negative incremental angles until the 2D gear teeth are fully formed, as shown in Figure 18. This study employs the SolidWorks interface as a platform to produce the 2D tooth shapes, as illustrated in Figure 19. This approach is effective for producing the 3D profiles of helical gear teeth. Figure 20 illustrates the 3D helical gear models used in this work to quantitatively examine the effect of contact stress at various locations on gear teeth.

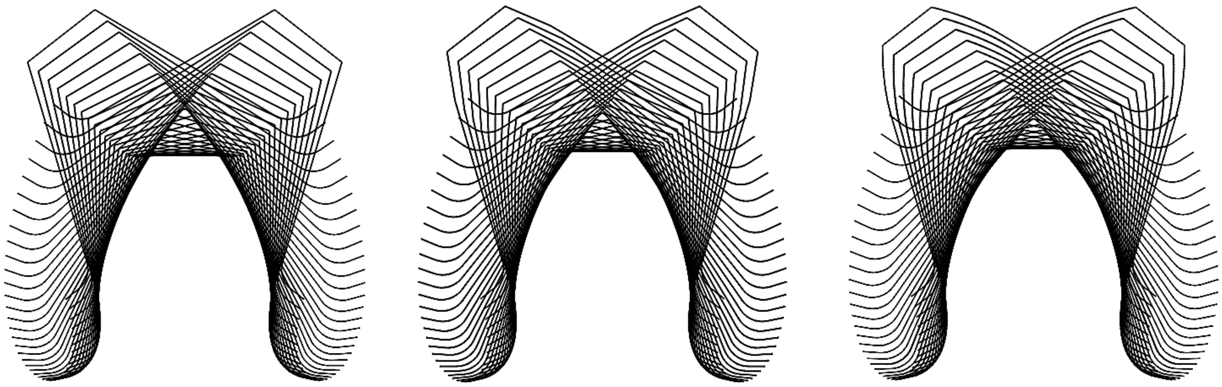

Standard tooth shape | Modified tooth shape with tip relief modification | Modified tooth shape with epicycloidal modification

Figure 18. Samples of the tooth shapes obtained using the QBASIC programming language

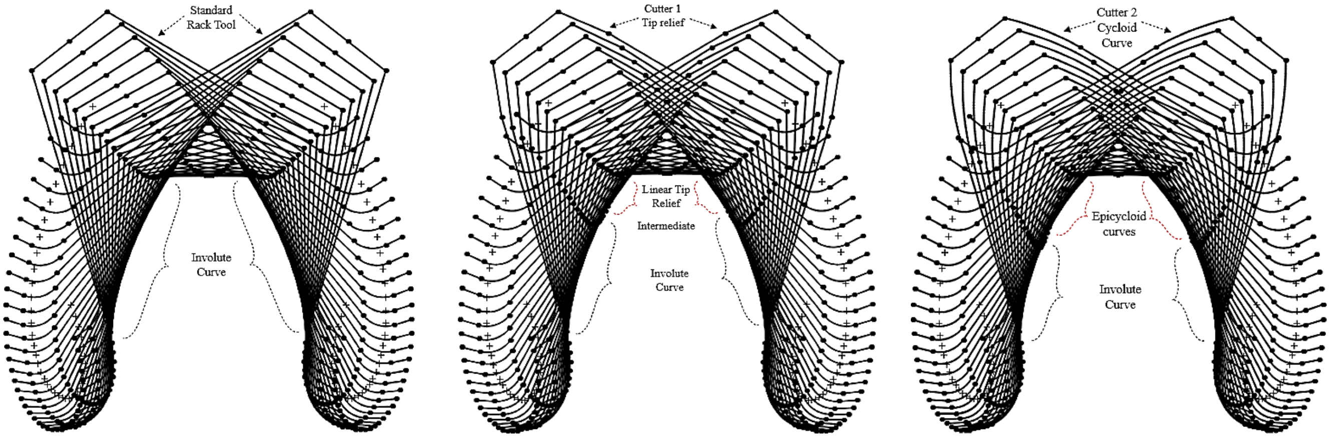

Standard tooth shape | Modified tooth shape with tip relief modification | Modified tooth shape with epicycloidal modification

Figure 19. Samples of the tooth shapes obtained using SolidWorks

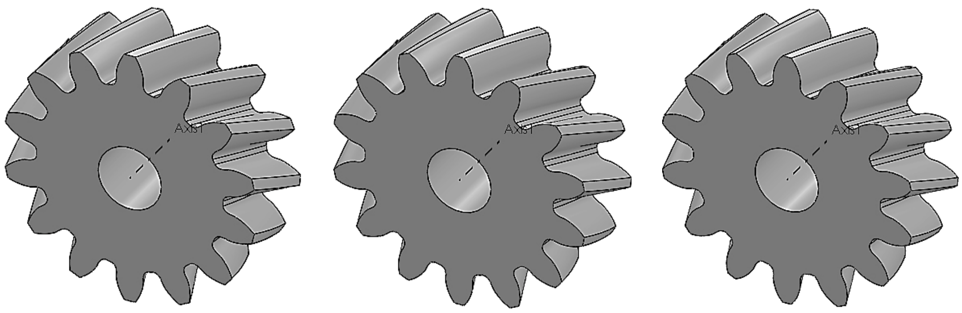

Figure 20. Three types of helical gear tooth surfaces: standard, with tip relief, and with epicycloid profiles

5.4 Sliding Velocity

The results of the sliding velocity for the two cases are shown in Figure 21, which presents a comparative analysis of the impact of the modified tooth geometry on the velocity of sliding. The maximum sliding rapidity magnitude appears near the contact points at certain angular positions, typically occurring just before and after the pitch point. Precise modifications are expected to reduce the sliding distance, thus decreasing the velocity at the moment of contact by implementing compounded modification.

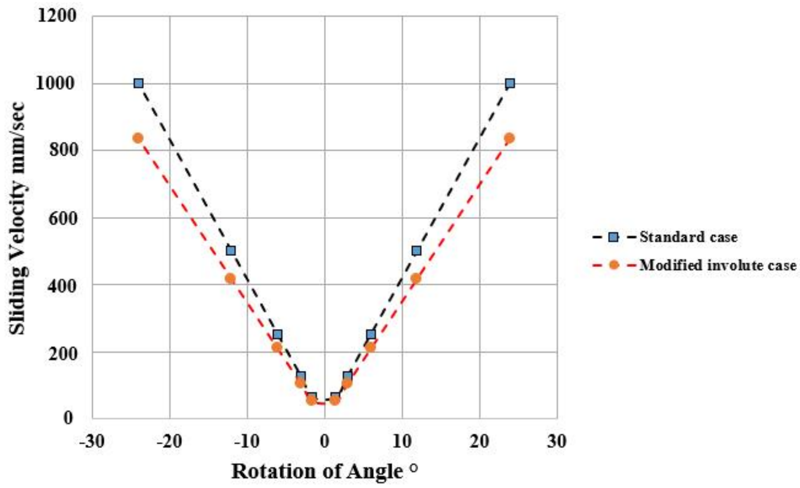

Figure 21. Comparison of sliding velocities for two scenarios with varying degrees of rotation

Table 1 presents the values of analytical sliding velocity for two crossed helical gears operating at different rotational angles. The results indicate the magnitude of peak velocity occurring at the contact position at a certain angular rotation. Naturally, maximum sliding occurs before and after the pitch point. The compound tooth modification reduces the sliding distance, thereby decreasing the velocity at the moment of contact. The enhancement percentage, in comparison to the standard case, is approximately 16%. This study demonstrates that the geometry of mated gears significantly influences the reduction of sliding velocity in the tooth contact regions, which can be affected by the shape and the contact area size. The increased contact area using the concave-convex flank option for the modified surface improves the contact ratio, reduces the heat friction, and increases the tooth thickness. Modifying the involute surface contributes to a reduction in the friction area. All these modifications have a substantial impact on improving the thermal performance of crossed helical gears, as well as reducing the stress experienced by the helical gears.

Table 1. The analytical results of sliding velocities in relation to rotation angles

Rotation Angle	Sliding Velocity of Standard Case (mm/sec)	Sliding Velocity of Modified Involute Case (mm/sec)	Enhancement Percentage (%)
24	1,000.02960	833.67120	16
12	500.01480	416.83560	16
6	250.00740	208.41780	16
3	125.00370	104.20890	16
1.5	62.50185	52.10445	16
-1.5	62.50185	52.10445	16
-3	125.00370	104.20890	16
-6	250.00740	208.41780	16
-12	500.01480	416.83560	16
-24	1,000.02960	833.67120	16

5.5 Contact Ratios

The results of the contact ratio, derived from Equation (45) for crossed helical gears, are presented in Tables 2 and 3. These tables present the relationship between the contact ratio with the pressure angle and the helix angle.

Table 2. The results of contact ratios for the intersecting helical gear system under the effect of different normal pressure angles (helix angle = 22.5°, module = 7 mm, and number of teeth = 14)

Pressure Angle	Transverse Contact Ratio	Axial Overlap Ratio	Total Contact Ratio
14.5°	1.308	0.208	1.516
20.0°	1.333	0.198	1.531
25.0°	1.225	0.168	1.393
30.0°	1.155	0.143	1.298

Table 3. The results of contact ratios for the intersecting helical gear system under the effect of different helix angles (pressure angle = 20°, module = 7 mm, and number of teeth = 14)

Helix Angle	Transverse Contact Ratio	Axial Overlap Ratio	Total Contact Ratio
15.0°	1.405	0.088	1.493
22.5°	1.333	0.198	1.531
30.0°	1.233	0.349	1.582
37.5°	1.108	0.539	1.647
45.0°	0.961	0.760	1.720

The relationships are depicted in Figures 22 and 23, which show that the contact ratio is enhanced by a reduced pressure angle and an increased helix angle. Therefore, it is beneficial to employ a low-pressure angle with a certain optimal helix angle. This configuration is considered one of the advantages of the characteristics of the helical gear system, as a higher contact ratio leads to the gradual engagement of crossed helical teeth, thereby contributing to a reduction in noise.

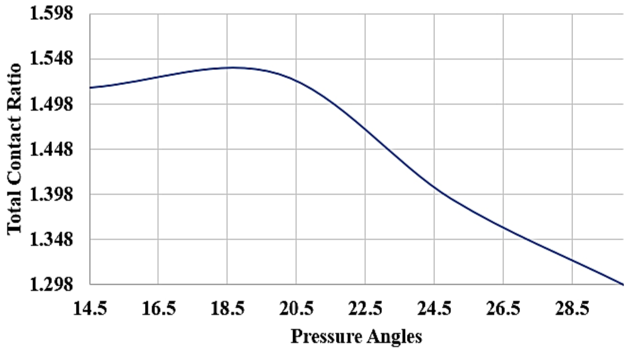

Figure 22. The correlation between the overall contact ratio and different pressure angles for crossed helical gears

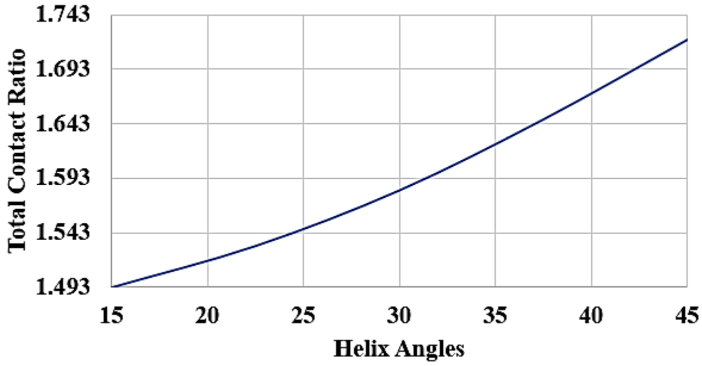

Figure 23. The correlation between the overall contact ratio and various helix angles for the crossed helical gear

5.5 Contact Stress Analysis

The analytical results have been presented to evaluate the contact stress and to estimate the dimensions of deformation during the simulation of the crossed helical gear system. These dimensions are directly related to the base circle on the loaded side regardless of other parameters determined by the computer software. The results are derived from analytical techniques, as defined in previous sections. The estimation of the contact shape and stress magnitude was conducted by using the MATLAB software package.

The maximum stress value, contact shape, and sliding velocity are influenced by the length of the action distance (H_1H_2) and the pressure tooth angle. Table 4 presents the contact stress values, half of the major and minor axes for the contact shape and the equivalent crossing angle that is closely aligned with the lines of action for a crossed helical teeth pair with an angle of 20° and corresponding lines of action. It is clear that the maximum stress values remain consistent across all cases, as they share the same length of action distance. An increase in the pressure angle decreases the curvature radius, as indicated in Equations (46 and 47), which in turn reduces the concentrated load on the area of contact between the two surfaces. Conversely, modification to the Hertz equation yields inverse results, where these changes affect the shape of the contact ellipse, resulting in a reduction of contact stress as both the pressure and helix angles increase.

Table 4. The analytical results of the effect of pressure angle and curvature radius on the contact stress values

α_n (°)	δ_p (mm)	a (mm)	b (mm)	$\boldsymbol{\lambda}$ (°)	ϑ (°)	μ (mm)	σ_c (MPa)
20	20.834	0.2897	0.00081	45	16.1268	41.6679	303.718

5.6 Finite Element Method

One numerical technique that might help provide a rough answer is finite element analysis. The analytical solution of various stress values in mechanical models is very complicated. Numerical results facilitate the measurement of the strength within the domain of the crossed helical gear teeth with appropriate boundary conditions [43]. The model is divided into elements under the procedure called discretization. The recommendations indicate the necessity of defining the governing equations for each element. Determining material properties, including thermal conductivity and material strength, is essential. Each element corresponds to a particular equation, which is combined to formulate the global equation for the mesh.

The behavior of the body is described as a whole. The global governing equation is expressed as follows:

$$[K]\{A\} = \{B\} \tag{66}$$

where $[K]$ is a singular matrix called the matrix of stiffness, $\{A\}$ is the freedom nodal degree, and $\{B\}$ is the nodal force of external. In this analysis, the contact field is considered to be non-linear, which requires a sophisticated software package to solve it. The models were developed using SolidWorks and subsequently exported to the ANSYS software package [44]. The design parameters for the three cases are shown in Table 5, which details the specific parameters associated with the crossed helical gear cases. The ANSYS software package was used to examine the contact problem. Figure 24 shows three types of meshing for crossed helical gears. To validate the final mesh density, a mesh convergence study was performed for three crossed helical gear teeth models as mesh convergence is required. Mesh sensitivity was also investigated using ANSYS. Figure 25 depicts the results of the mesh convergence test. The nodes of the mesh were determined according to the tooth surface equations, as previously mentioned.

The structural material employed in this study is steel, characterized by Young's modulus of 207 GPa and a Poisson's ratio of 0.299. A power input of 20 kW at 1,440 rpm was applied for all crossed helical gear units. During the rotational operation of the helical gears, each tooth will share the load. Both double-tooth and single-tooth contacts are considered. Therefore, the contact ratio is a crucial component in this study. The angle of rotation was divided into any desired angular periods. One pair of helical teeth is in contact at a crossing angle of 45°. Various contact scenarios were analyzed based on the previous formulation. This study examined three contact positions for the crossed helical gear models: at a pitch point and rotation angles of 5° and 10°. The contact stress values for the three cases were compared. Different contact positions influence the modifications on the standard tooth surface.

Table 5. The parameters of the crossed helical gear and pinion cases

Cases	Crossing Angle, λ (°)	Module, m_n (mm)	Pressure Angle, α_n (°)	Helix Angle, β_p (°)	Face Width, F (mm)	No. of Teeth, Z	Radius of Circle Generations, R (mm)	Amount of Tip Relief, msl (μmm)	Length of Tip Relief, ℓ (mm)
1	45	7	20	22.5	40	14	-	-	-
2	45	7	20	22.5	40	14	-	60	3.56
3	45	7	20	22.5	40	14	9	-	-

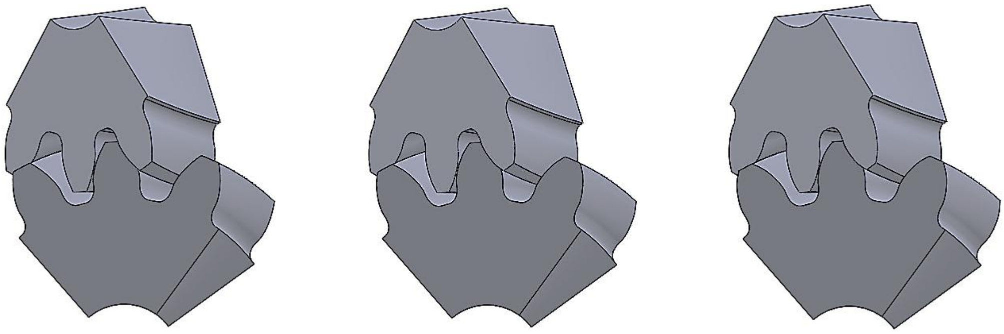

Figure 24. The standard design, the tip relief modification, and the epicycloidal modification of crossed helical gears at a crossing shaft angle of 45°

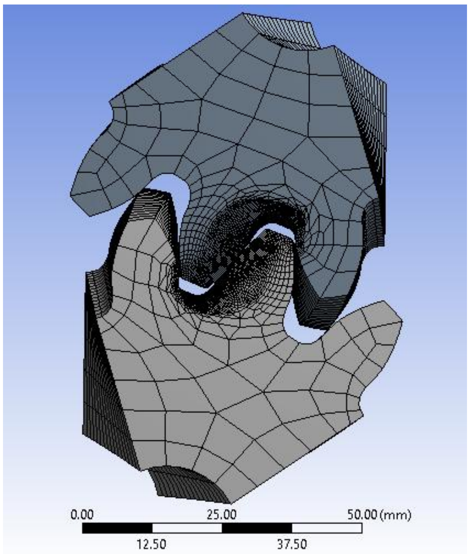

Figure 25. Three-dimensional model of a crossed helical gear tooth mesh

In this section, various results are presented to evaluate the performance of crossed-standard and non-standard helical gear systems. These results are based on the numerical method (i.e., FEM) from the analysis conducted using ANSYS Simulation Mechanical to estimate contact stress. The maximum stress of contact and the cumulated stress of the tooth root region of the crossed helical gear teeth were calculated using ANSYS. Three models, each featuring three teeth, were prepared for this study. Table 6 displays the stress results for three positions across the three gear models at a specified coefficient of friction. The friction coefficient varies from approximately 0.05 to 0.25, depending on the ambient conditions. This research used a coefficient value of 0.05 to evaluate gear performance. Two images depicting the three sets of intersecting models at three locations illustrate the peak contact and root stresses, along with their contact ellipses, locations, and intensities. The comparison reveals that the contact stress exhibits a point contact that transforms into an ellipse, with the stress concentrated in the tooth root region. The contact stress is represented by the equivalent von Mises stress at three positions: once at the pitch point, near the tip point, and in the region between them. The maximum contact stress occurs at the pitch point due to the high instantaneous contact between teeth meshing, which subsequently decreases near the tip position. The effect of modification on the performance of crossed helical gear teeth includes an enhancement of contact stress and a reduction in root stress due to the helix angle.

Table 6. The maximum contact stress and fillet tooth root stress at three positions for three gear models

Contact Location	Standard Case	
Pitch Point	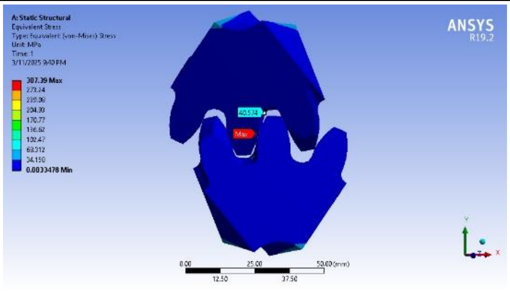	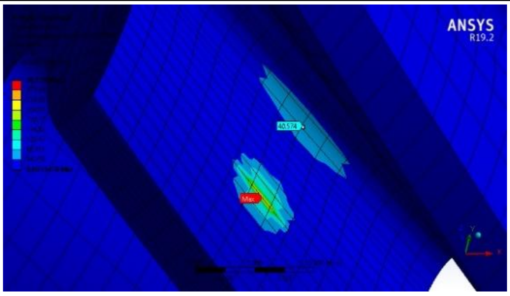
5°	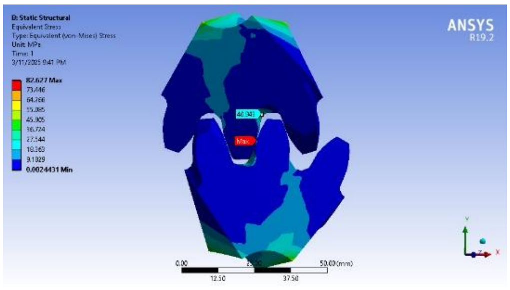	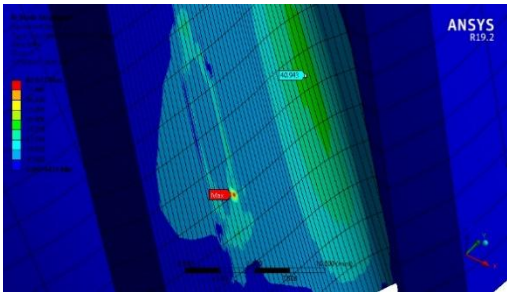
10°	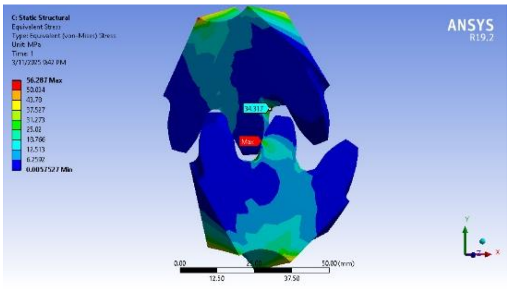	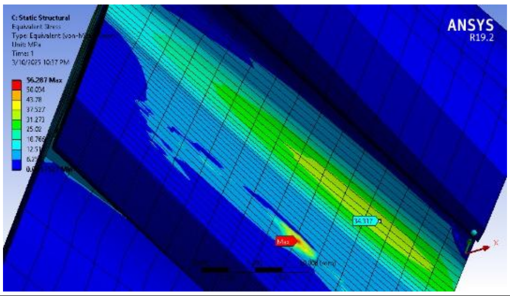
Contact Location	**Modified Involute Case**	
Pitch point	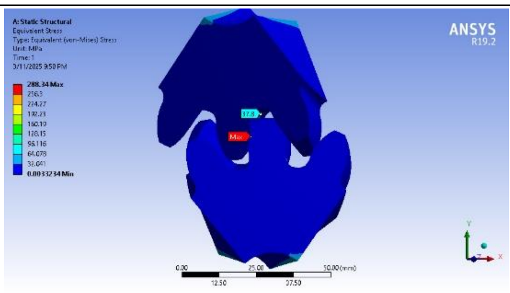	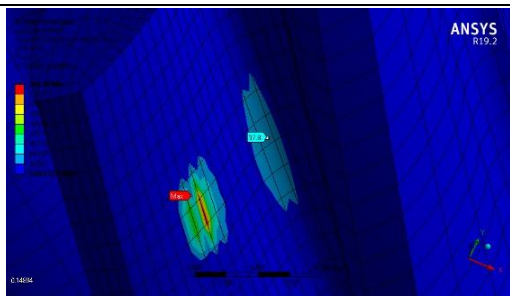
5°	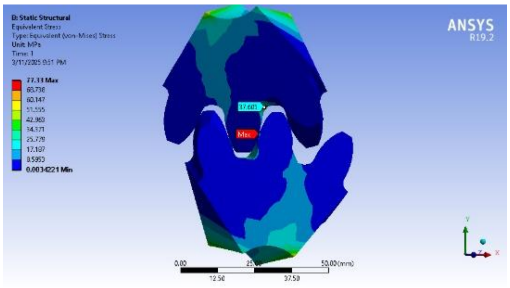	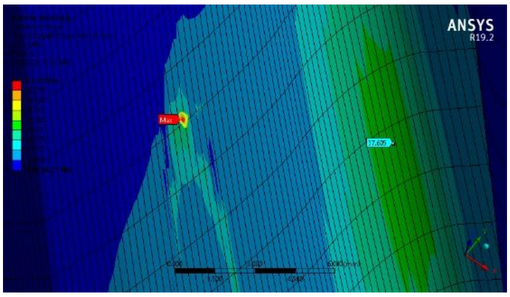
10°	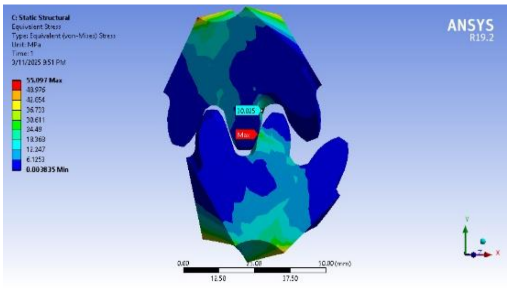	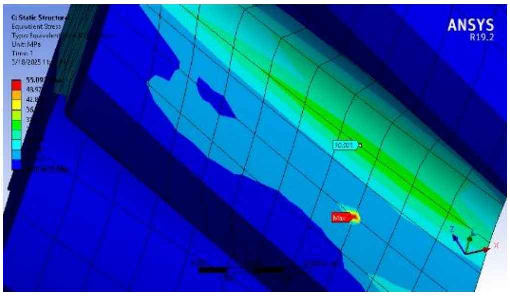

Table 7 presents the results of von Mises stress values, while Table 8 provides the results of the stress inside the root area for all gear models across the three contact positions. Figures 26 and 27 illustrate the relationship between the contact stress and the tooth root stress region with three contact positions, respectively.

Table 7. The numerical results of von Mises stress values

Position	Contact Stress, σ_c (MPa)		Enhancement Percentage	Contact Stress, σ_c (MPa)	Enhancement Percentage
	Standard Gears	With Tip Relief Modification		With Epicycloidal Modification	
Pitch Point	307.390	298.770	2%	288.340	6%
At 5° Angle of Rotation	82.623	77.618	6%	77.330	6%
Near Tip Point	56.287	59.690	-6%	55.097	2%

Table 8. The numerical results of the stress inside the tooth root region

Position	Stress Inside the Tooth Root Region, σ_b (MPa)		Enhancement Percentage	Stress Inside the Tooth Root Region, σ_b (MPa)	Enhancement Percentage
	Standard Gears	With Tip Relief Modification		With Epicycloidal Modification	
Pitch Point	40.574	39.716	2%	37.800	6%
At 5° Angle of Rotation	40.943	38.065	7%	37.605	8%
Near Tip Point	34.287	34.809	-1%	30.025	12%

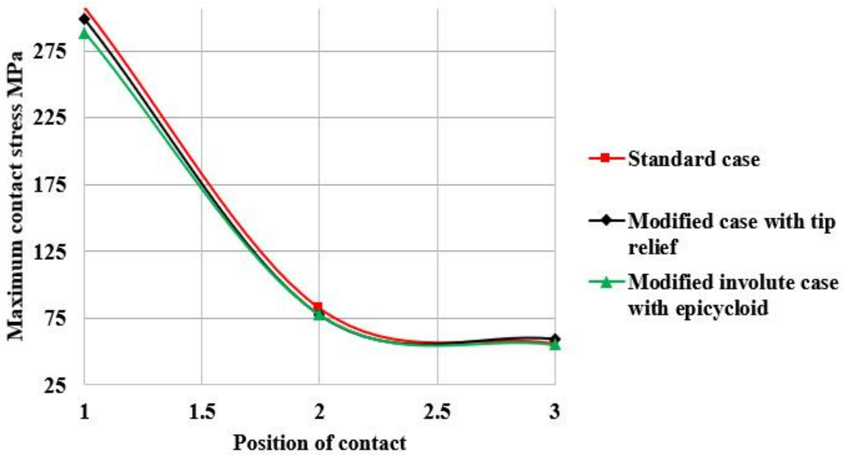

Figure 26. The relationship between contact stress and three contact positions

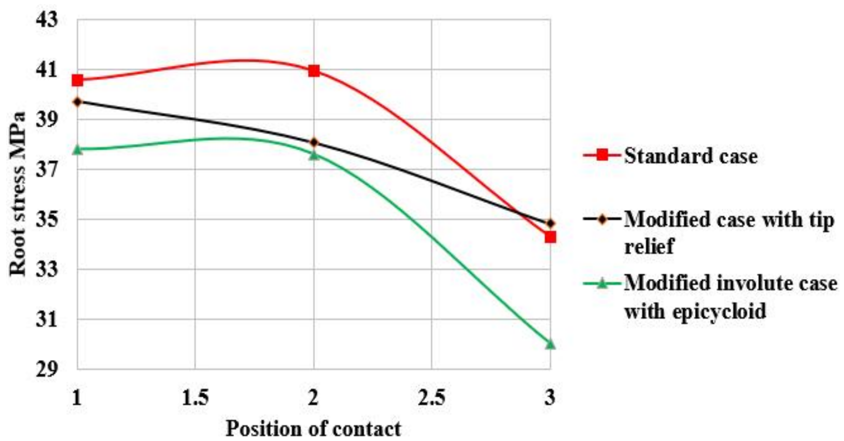

Figure 27. The relationship between the tooth root stress and three contact positions

Tables 7 and 8 indicate a notable enhancement in the performance of the crossed helical gear unit featuring teeth with tip relief modification in comparison to the standard crossed helical gear. The contact points are identified at the pitch point, near the tip point, and between them. The percentage enhancement in maximum contact stress is 2%, 6%, and -6%, respectively, while the percentage enhancement in the tooth root stress area is 2%, 7%, and -1%, respectively. In the final position, there is no significant difference between both stress cases. Furthermore, the crossed helical gear unit featuring teeth subjected to epicycloidal modification demonstrates enhancements when compared to the standard gear unit. The contact points are identified at the pitch point, near the tip point, and between them. The percentage enhancement in maximum contact stress is 6%, 6%, and 2%, respectively, while the percentage enhancement in the tooth root stress area is 6%, 8%, and 12%, respectively.

Figures 27 and 28 depict a reduction in contact stress as the contact point moves away from the pitch point toward the tip of the tooth. Moreover, the stress inside the root region decreases when the contact point is far from the pitch point. These improvements in tooth contact and tooth root stress area, resulting from the implementation of the first and second proposed tooth modifications, are attributed to the improved ability of the helical tooth profile. This enhancement leads to increased resistance against higher loads, improved gear durability, reduced impact forces during engagement, and the mitigation or elimination of interference. The stress concentration factor K_t is crucial in gear design, as it represents the ratio of the numerical value to the analytical value. The determination of the stress concentration factor for both the standard and the current crossed helical gear systems depends on the results of the contact stress analysis. The following formula is used to evaluate the value of the stress concentration factor:

$$K_t = \frac{\sigma_{c_{max}}}{\sigma_{c_{mon}}} \tag{66}$$

The results for the stress concentration factor K_t are presented in Table 9. These data pertain to the standard crossed helical gear case. The findings suggest that the implementation of modified helical teeth reduces the stress concentration factor, hence mitigating abrupt changes in the cross-sectional tooth area subjected to stress, which results in reduced stress concentration.

Table 9. The stress concentration factor and the enhancement percentage in relation to the standard crossed helical gear case

Cases	K_t	Enhancement Percentage
Standard Teeth	1.01	---
Modified Helical Teeth with Tip Relief	0.98	2%
Modified Helical Teeth with Epicycloid	0.94	6%

According to this research, the shape of the coupled gears is more important in reducing friction at the tooth contact areas. It is sensitive to the dimensions and the form of the contact area. By evaluating the scuffing surface, the contact and root stresses can be assessed to determine the level of friction experienced. Regarding surface scuffing, the novel conjugated crossed helical tooth profiles have demonstrated superior effectiveness. The compounded curves of the tip relief-involute or epicycloid-involute modifications serve to decrease the sliding distance. The friction generated between these surfaces over this distance is influenced by the nature of the contact. Tip relief modification is designed to reduce the impact shock of the contact at the moment of initial engagement. Furthermore, an involute surface has been modified to be shorter than that of a standard surface. The epicycloid region is characterized by a high contact ratio, attributable to its conformal geometry.

6. CONCLUSION

The shaping process is a suitable simulation for the modification of helical gear teeth. In this study, a new technical method was used to draw traditional involute and non-involute helical teeth, utilizing the SolidWorks interface as a platform for generating 3D profiles of helical gear teeth. The involute-epicycloid profile designed for a crossed helical gear reduces the sliding distance, thus lowering the velocity at the moment of contact when compared to a standard crossed helical gear. The enhancement percentage is approximately 16%. The contact ratio improved through a reduction in the pressure angle and an increase in the helix angle. The total contact ratios are 1.5 and 1.7, respectively. A higher contact ratio leads to the gradual engagement of crossed helical teeth, which helps to reduce the noise. The transmission error decreases by increasing the amount of misalignment, resulting in a smaller harmonic waveform. The most significant improvement in the crossed helical gear is the epicycloidal modification of the gear teeth along the loaded side, in comparison to a standard gear case. For epicycloidal modification, the enhancement percentage in maximum contact stress is 6%, 6%, and 2%, while the enhancement percentage in the tooth root stress area is 6%, 8%, and 12%. On the other hand, for tip relief modification, the enhancement percentage in maximum contact stress is 2%, 6%, and -6%, while the enhancement percentage in the tooth root stress area is 2%, 7%, and -1%. The stress concentration factor decreased through the application of modified helical teeth, with enhancement percentages reaching 2% and 6% when utilizing tip relief and non-involute modification, respectively. The results indicate that a modified crossed helical gear drive exhibits superior performance compared to a standard gear drive for a given helix angle.

ACKNOWLEDGEMENT

The authors would like to express their sincere gratitude to all staff members of the Mechanical Engineering Department at the College of Engineering, University of Baghdad, for their cooperation and support during the preparation of this work.

CONFLICT OF INTEREST

The authors declare that they have no known competing financial interests or personal relationships that could have appeared to influence the work reported in this paper.

AUTHORS CONTRIBUTION

Mohammed Abdulaal Kadhim: Ideas, Techniques, Programs, Research, and Writing - Original Copy.

Mohammad Qasim Abdullah: Conceptualization, Supervision, Composition - Original Draft.

REFERENCES

[1] J. J. Uicker Jr, G. R. Pennock, and J. E. Shigley, Theory of machines and mechanisms, 6th ed., Cambridge University Press, 2023.

[2] W. A. Altabey, Fundamentals of Machine Component Design, 4th ed., Elsevier, 2023.

[3] S. S. Rattan, Theory of machines, 4th ed., Tata McGraw-Hill Education, 2014.

[4] S. Sankar and M. Nataraj, "Prevention of helical gear tooth damage in wind turbine generator: a case study," *Proceedings of the Institution of Mechanical Engineers, Journal of Power and Energy*, vol. 224, no. 8, pp. 1117-1125, 2010.

[5] N. Seyama, K. Nagamura, and K. Ikejo, "Design of Involute-Cycloid Composite Tooth Profile Spur Gear to Reduce the Influence of Center Distance Error on Driving Performance," Dept. of Mechanical System Engineering, Graduate School of Hiroshima University, Kagamiyama 1-4-1, Higashi-Hiroshima, Hiroshima, pp. 739-8527, Japan, 2011.

[6] X. Zhang and Z. Liang, "Comparison of conventional double-helical and curvilinear cylindrical gear drives in terms of transmission errors and stress," *Transactions of FAMENA*, vol. 45, no. 3, pp. 1-18, 2021.

[7] D. Liang, S. Meng, and R. Tan, "Mathematical model and characteristics analysis of crossed-axis helical gear drive with small angle based on curve contact element," *Science Progress*, vol. 104, no. 2, pp. 1-19, 2021.

[8] J. Wu, P. Wei, C. Zhu, P. Zhang, and H. Liu, "Development and application of high strength gears," *The International Journal of Advanced Manufacturing Technology*, vol. 132, no. 7, pp. 3123-3148, 2024.

[9] M. Abdulaal and M. Q. Abdulah, "Mathematical model and generation analysis for crossed helical gear system," *World Journal of Engineering*, 2024.

[10] M. Q. Abdullah and M. A. Kadum, "Stress concentration factor analysis of helical gear drives with asymmetric teeth profiles," *Journal of Engineering*, vol. 24, no. 5, pp. 14-28, 2018.

[11] M. A. Kadhim and M. Q. Abdullah, "Generation and stress analysis of helical gear tooth combining involute with epicycloidal and hypocycloidal profiles," *International Journal of Automotive and Mechanical Engineering*, vol. 22, no. 1, pp. 12016-12034, 2025.

[12] X. Zheng, W. Zhu, G. Li, and Y. Hu, "Reshaping load-dependent mesh excitation waveforms of spur gears—an analytical framework on tip relief modeling and design," *Machines*, vol. 13, no. 2, p. 161, 2025.

[13] C. Liu, K. Ouyang, T. Jiang, and C. Liu, "Fracture failure analysis of gear teeth," *Journal of Physics: Conference Series, International Conference on Applied Mechanics and Structural Materials*, Nanjing, vol. 2206, no. 1, p. 012036, 2021.

[14] A. Jung, *Machine Learning: The Basics*, Springer Singapore, 1st ed., 2022.

[15] R. R. Craig and E. M. Taleff, *Mechanics of Materials*, 4th ed. New York: John Wiley and Sons, 2020.

[16] K. H. Grote and H. Hefazi, *Springer Handbook of Mechanical Engineering*, 2nd ed., Springer Singapore, 2021.

[17] D. T. Babichev and N. A. Barmina, "Computer-aided design of gears and machine-tool meshing with application of new concepts, images and indices," *New Approaches to Gear Design and Production*, pp. 157-185, 2020.

[18] F. L. Litvin, Q. Fan, D. Vecchiato, A. Demenego, R. F. Handschuh, and T. M. Sep, "Computerized generation and simulation of meshing of modified spur and helical gears manufactured by shaving," *Computer Methods in Applied Mechanics and Engineering*, vol. 190, no. 39, pp. 5037-5055, 2001.

[19] Z.-G. Wang, Y.-C. Chen, "Design of a helical gear set with adequate linear tip-relief leading to improved static and dynamic characteristics," *Mechanism and Machine Theory*, vol. 147, p. 103742, 2020.

[20] Fuentes-Aznar, S. E. Gonzalez-Perez, "Computerized Simulation of Manufacturing Errors in Cylindrical Spur Gears and Their Compensation Through Flank Modifications Mechanisms and Machine Science," In: Goldfarb, V., Trubachev, E., Barmina, N. (eds) Advanced Gear Engineering., vol 51. Springer, pp. 1-25, 2018.

[21] X. Xu, Y. L. S. Zuo, P. Tenberge, P. Dong, Y. Liu et al., "A novel tooth tip relief method for reducing micro-pitting of spur gears," *Advances in Mechanical Engineering*, vol. 13, no. 9, 2021.

[22] M. Temirkhan, H. B. Tariq, K. Kaloudis, C. Kalligeros, V. Spitas, and C. Spitas, "Parametric quasi-static study of the effect of misalignments on the path of contact, transmission error, and contact pressure of crowned spur and helical gear teeth using a novel rapidly convergent method," *Applied Sciences*, vol. 12, no. 19, p. 10067, 2022.

[23] T. Stolarski, Y. Nakasone, and S. Yoshimoto, *Engineering analysis with ANSYS software*, 2nd ed., Butterworth-Heinemann: Springer, 2018.

[24] J. D. Smith, *Gear noise and vibration*, 2nd ed., Boca Raton: CRC Press, 2003.

[25] J. Denavit, R. S. Hartenberg, "A kinematic notation for lower-pair mechanisms based on matrices," *Applied Mechanics*, vol. 22, no. 2, pp. 215-221, 1955.

[26] S. Luo, M. Jingyu, "Manufacturing and contact characteristics analysis of a novel 2K-H internal meshing planetary reducer with involute-cycloid combined tooth profiles," *Mechanical Engineering Science*, vol. 238, no. 13, pp. 6706-6724, 2024.

[27] N. Seyama, K. Nagamura, K. Ikejo, and K. Isaki, "GSD-05 Influence of design parameters on strength and driving performance of involute-cycloid composite tooth profile gears (gear strength and durability, including gear materials and heat treatment techniques)," in *The Proceedings of the JSME International Conference on Motion and Power Transmissions 2009*, The Japan Society of Mechanical Engineers Pages: 329-332, 2009.

[28] S. P. Radzevich, M. Storchak, Advances in gear theory and gear cutting tool design, 1st ed., Switzerland: Springer Cham, 2022.

[29] S. Glodež, Gear geometry, Elsevier, pp. 59-92, 2025.

[30] V. Abadjiev, E. Abadjieva, "Geometric Pitch Configurations–Basic Primitives of the Mathematical Models for the Synthesis of Hyperboloid Gear Drives.," In: Goldfarb, V., Trubachev, E., Barmina, N. (eds) Advanced Gear Engineering. Mechanisms and Machine Science, vol 51. Springer, Cham., 2018.

[31] A. A. Shabana, "Analysis of involute-curve geometry using position gradients: Application to gear-tooth profile," *Mechanics Based Design of Structures and Machines*, vol. 52, no. 12, pp. 10723-10745, 2024.

[32] R. C. Juvinall, K. M. Marshek, Fundamentals of machine component design, 5th ed., New York: John Wiley and Sons, 2020.

[33] H. A. Zschippang, S. Weikert, K. Wegener, "Face-gear drive: Meshing efficiency assessment," *Mechanism and Machine Theory*, vol. 171, p. 104765, 2022.

[34] A. L. Kapelevich, Direct gear design, 2nd ed., Boca Raton: CRC Press, 2021.

[35] E. K. Browning, M. A. Zupan, Microeconomics: Theory and applications, 13th ed., New York: John Wiley and Sons, 2020.

[36] L. Becker, P. Tenberge, "Crossed helical gears—simulative studies and experimental results on non-involute geometries," Forschung im Ingenieurwesen, vol. 87, no. 3, pp. 949-959, 2023.

[37] O. D. Mohammed, "An analytical approach for the determination of helical gear tooth geometry," *Journal of Engineering*, Design and Technology, vol. 22, no. 6, pp. 2020-2042, 2024.

[38] N. Gaoxiang, S. Chaosheng, F. Zifan, Z. Zhang, "Effects of geometric design parameters and misalignments on contact ellipse of crossed beveloid gears," *Mechanism and Machine Theory*, vol. 165, no. 104441, pp. 1-20, 2021.

[39] Victor R. Casanova, I. G. Perez, "Investigation of the effect of contact pattern design on the mechanical and thermal behaviors of plastic-steel helical gear drives," *Mechanism and Machine Theory*, vol. 164, no. 104401, pp. 1-20, 2021.

[40] E. Tamuta, R. Nemoto, H. Tomita, E. Tanaka, H. Takahashi, "Contacting State on Imaginary Rack of Crossed Helical Gears," in *The 3rd International Conference on Design Engineering and Science, ICDES 2014*, Pilsen, Czech Republic, August 31 – September 3, 2014, 2014.

[41] E. Tamura, R. Nemoto, N. Seyama, E. Tanaka, "Contact Stress State of Crossed Helical Gears," in *The 4th International Conference on Design Engineering and Science, ICDES 2017*, Aachen, Germany, September 17-19, 2017.

[42] F. L. Litvin, I. G. Perez, A. Fuentes, D. Vecchiato, and T. M. Sep, " Generalized concept of meshing and contact of involute crossed helical gears and its application," *Computer Methods in Applied Mechanics and Engineering*, vol. 194, no. 34–35, p. 3710-3745, 2005.

[43] P. M. Ramachandra, S. Sutar, G. M. Kumara, "Stress analysis of a gear using photoelastic method and finite element method: Review," *Materials Today: Proceedings*, vol. 65, no. 8, pp. 3820-3828, 2022.